Analog for Fluvial-Deltaic Reservoir Modeling: Ferron Sandstone of Utah
AAPG Studies in Geology 50
T.C. Chidsey, Jr., R.D. Adams, and T.H. Morris, editors

Sedimentology and Structure of Growth Faults at the Base of the Ferron Sandstone Member Along Muddy Creek, Utah

Janok P. Bhattacharya[1] and Russell K. Davies[2]

ABSTRACT

This paper describes normal growth faults at the base of the Ferron Sandstone exposed along the highly accessible walls of Muddy Creek Canyon in central Utah. Although there have been several studies of growth faults in outcrops this is the first that integrates detailed sedimentological measured sections with fault kinematics and section restorations. We measured 20 sedimentological sections and interpreted a photomosaic covering approximately 200 m (550 ft) lateral distance. The outcrop is oriented parallel to depositional dip and perpendicular to the general strike of the faults.

Distinctive pre-growth, growth, and post-growth strata indicate a highly-river dominated crevasse delta, that prograded northwest into a large embayment of the Ferron shoreline. The growth section comprises medium-to large-scale cross stratified sandstones deposited as upstream and downstream accreting mouth bars in the proximal delta front. Deposition of mouth bar sands initiates faults. Because depositional loci rapidly shift, there is no systematic landward or bayward migration of fault patterns. During later evolution of the delta, foundering of fault blocks creates an uneven seafloor topography that is smoothed over by the last stage of deltaic progradation.

Faults occur within less than 10 m (30 ft) water depths in soft, wet sediment. Detailed examination of the fault zones shows that deformation was largely by soft-sediment mechanisms, such as grain rolling and by lubrication of liquefied muds, causing shale smears. Mechanical attenuation of thin beds occurs by displacement across multiple closely spaced small throw faults.

Analogous river-dominated deltaic subsurface reservoirs may be compartmentalized by growth faults, even in shallow-water, intracratonic, or shelf-perched highstand deltas. Reservoir compartmentalization would occur where thicker homogenous growth sandstones are placed against the muddy pre-growth strata and where faults are shale-smeared, and thus potentially sealing.

[1]*Geosciences Department, University of Texas at Dallas, Richardson, Texas*
[2]*Rock Deformation Research, USA Inc., McKinney, Texas*

INTRODUCTION

Synsedimentary normal faults, or growth faults, associated with deltas are involved in the formation of major traps for oil and gas reservoirs and they may isolate compartments in subsurface hydrocarbon reservoirs or aquifers (Busch, 1975; Galloway et al., 1982; Bishop et al., 1995; Diegel et al., 1995). Subsurface studies of growth faults typically are based on seismic data, which are useful for mapping and describing regional-scale geologic architecture of growth faults, but not as useful for imaging finer-scaled details. Well log and core data invariably alias smaller scale structures. Outcrops, in contrast, can provide complete information about the lateral variability of growth-faulted strata and fault geometries at a range of scales. Because of the self-similarity of many structural styles at different scales, knowledge about growth faults at the outcrop scale may be applied to regional-scale growth fault systems.

Although there have been several studies of growth faults in outcrops (Brown et al., 1973; Edwards, 1976; Rider, 1978; Elliot and Lapido, 1981), there are no studies that integrate detailed sedimentological measured sections with fault kinematics and section restorations. The best-studied examples include beautifully exposed, but rather inaccessible Carboniferous-age growth strata along the sea-cliffs of Western Ireland (Rider, 1978, Elliot and Lapido, 1981) and Triassic and Cretaceous sea-cliff exposures along the Norwegian coast (Edwards, 1976; Nemec et al., 1988).

This paper describes the detailed sedimentology and structure associated with normal growth faults at the base of the Ferron Sandstone exposed along the highly accessible walls of Muddy Creek Canyon in central Utah (Figures 1 and 2). A prior study of these faults suggested that fault displacement was accommodated by movement of underlying mobile prodelta muds (Nix, 1999; Morris and Nix, 2000). This earlier study interpreted the fault style and broad stratigraphic relationships from photomosaics, but did not incorporate any detailed sedimentological measured sections. Our study provides a more detailed description of the interrelationship between the stratigraphy and structure.

Regional Stratigraphy and Paleogeography

The Ferron Sandstone is a fluvio-deltaic clastic wedge deposited near the end of the Sevier Orogeny into a rapidly and asymmetrically subsiding foreland basin that rimmed the western margin of the Late Cretaceous (Turonian) seaway in central Utah (Gardner, 1995, and this volume). The Ferron consists of seven regressive-transgressive stratigraphic cycles, each bounded by a flooding surface and associated coals (Ryer, 1984;

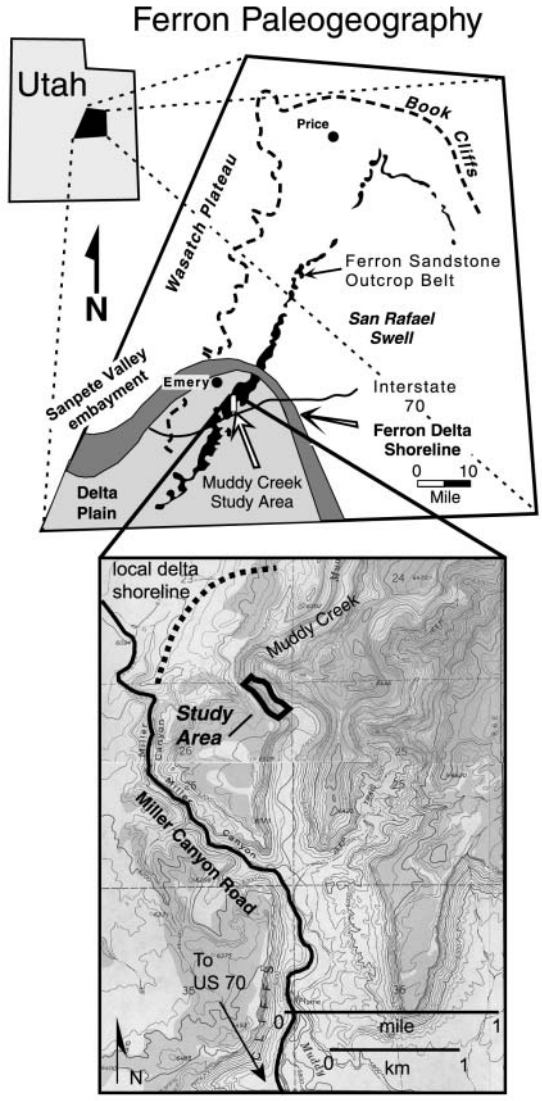

Figure 1. (A) Regional paleogeographic base map. In the Muddy Creek study area the delta lobe prograded locally to the northwest into the Sanpete Valley embayment (from Ryer and McPhillips, 1983). (B) Topographic inset with location of photomosaic along south cliff face of Muddy Creek as well as orientation of shoreline associated with northwest prograding bay-fill, crevasse delta lobe.

Gardner, 1995; Anderson and Ryer, this volume). In outcrop, the clastic wedges are exposed in sandstone cliffs above slope-forming mudstones (Figure 2).

Regionally, the Ferron is mapped as a large lobate body that prograded northwest, north, and northeast forming a large western embayment (the Sanpete Valley embayment in Figure 1) of the Cretaceous seaway (Ryer and McPhillips, 1983). Facies descriptions (see "stratigraphy and facies" section below) show that this bay experienced diminished wave activity compared to most of the Ferron Sandstone and was infilled with river-dominated delta lobes (Figure 3). This study focuses on one river-dominated delta lobe that built-out towards the northwest at a high angle to the regional progradation direction. This lobe may represent a large bay-fill

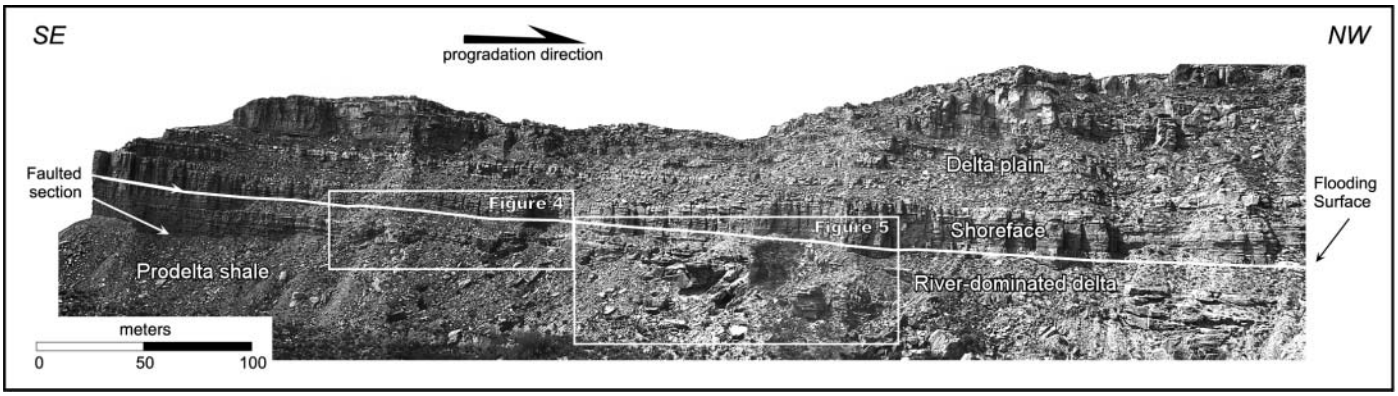

Figure 2. Panoramic photo of south cliff-face along Muddy Creek (located in Figure 1B) showing location of interpreted panels (Figure 4 – left; Figure 5 – right). Northwest dipping beds in unfaulted strata at the southeast end of the outcrop reflect inclined delta front sandstone beds. Closeup of this area is shown in Figure 8.

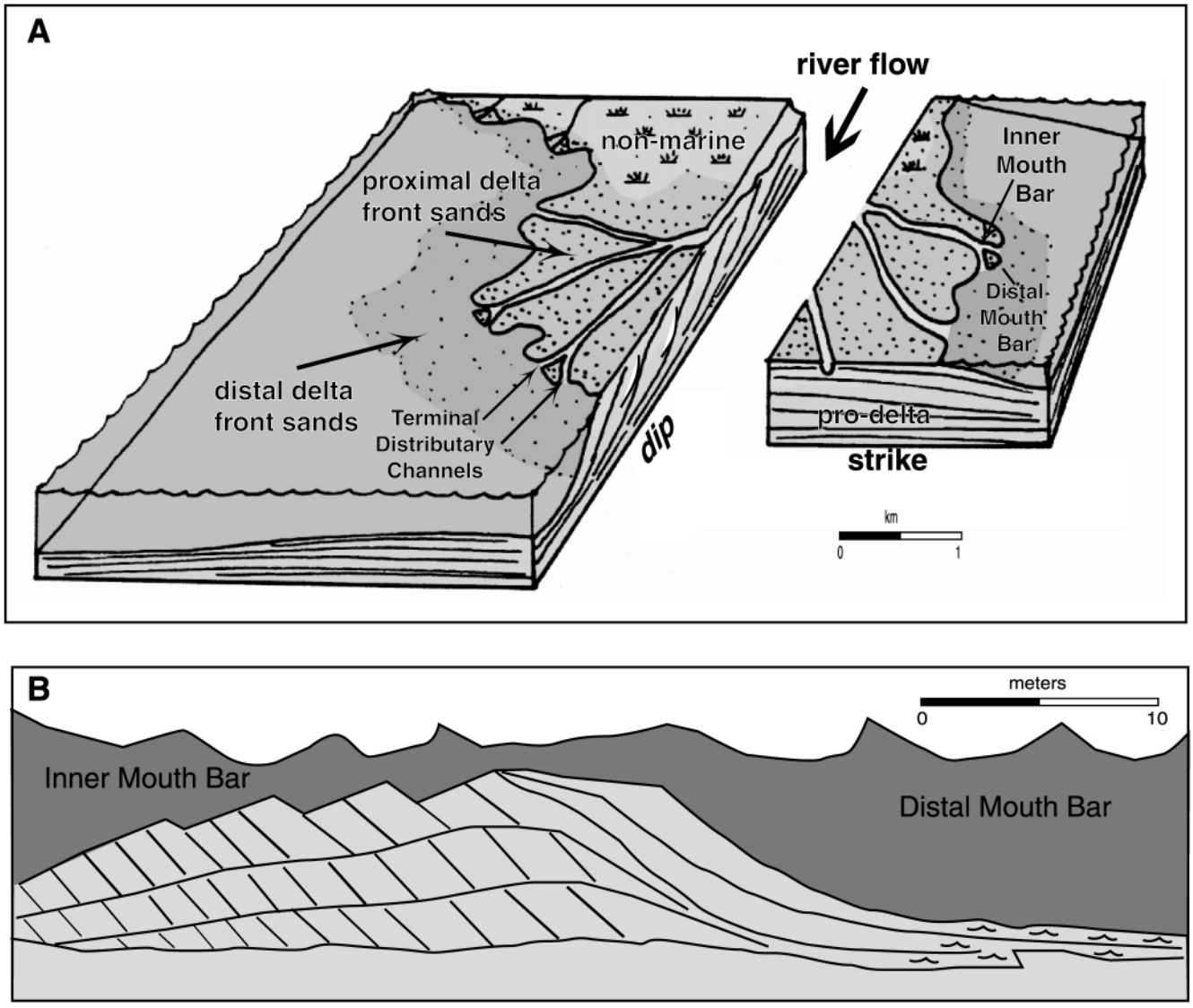

Figure 3. (A) Block diagram of a river-dominated, shoal-water delta showing position of inner and distal (outer) mouth bar deposits associated with the delta front. Lobate geometry reflects river dominance. (B) Schematic cross section of a distributary mouth bar, based on the Ferron example. Inner-mouth bar is characterized by movement of subaqueous dune-scale bedforms. Decreasing flow velocities cause upstream accretion of the bar. At the distal end of the bar, sands flow down the bar foreset and are locally reworked by waves.

crevasse delta associated with avulsion of the Ferron distributary channel system into this low area (see Moiola et al., this volume). We use the terms proximal and distal to refer to the southeast and northwest position associated with the landward and bayward progradation of this crevasse delta, rather than the more general southwest to northeast trend associated with progradation of the entire Ferron clastic wedge.

The lower portion of the Ferron has been associated with a minor drop of sea level within "short-term stratigraphic cycle 1" at the base of the "Ferronensis Sequence" of Gardner (1995). This sea-level drop may have forced the deposition of delta front and prodelta mudstones onto highly bioturbated older "shelf" mudstones of the underlying Tununk Shale Member of the Mancos Shale. Listric normal faults sole into this shale and growth of the section across the faults seems to occur exclusively within the delta front sands. It is the faults in this lower section that were mapped and are described in this paper.

Study Area

The mapped set of growth faults are well exposed on the southwest face of a 50 m (160 ft) high cliff along Muddy Creek canyon (Figures 1 and 2) and cover a 200 m (650 ft) lateral section near the base of the cliff. The faults are restricted to a 15-20 m (50-65 ft) section of prograding delta sands above the mud-rich pro-delta Tununk shale and below a flooding surface that separates the faulted delta sands from the thick overlying unfaulted strata of Ferron stratigraphic cycle 2. Faults are also exposed across the valley in the northeast cliff-face and along other meanders in the Muddy Creek Canyon and in adjacent creeks. This study focuses only on the faults in the southwest cliff of Muddy Creek.

Although the faults form a continuous set of structures across the face of the outcrop, for convenience we separate the description and discussion into a distal and proximal fault exposure. The proximal fault exposure extends from the southeast, unfaulted landward extension of the delta complex towards the central northwest bayward prograding and faulted section (Figure 2). The distal fault exposure extends from the center of the mapped fault set to the most bayward-mapped exposure (Figure 2). The exposure in both the proximal and distal fault sets is excellent over the thick clastic growth sections, but poor or covered in the underlying heterolithic more mud-rich section.

Methodology

We measured 20 sedimentological sections and interpreted a photomosaic covering the 200 m (650 ft) lateral distance over the exposed outcrop (Figures 4 and 5). Paleocurrent data and fault strike and dip data show that the cliff face studied is oriented parallel to the depositional dip of the delta lobe and perpendicular to the general strike of the growth faults (Figure 6).

Integrating facies and structure, we documented offset of specific beds across the faults. Distinctive facies geometry allowed us to determine the pre-growth, growth, and post-growth stratigraphy. These distinctive beds are characterized by specific grain sizes, sedimentary structures and stacking order, and are designated with different colors (see compact disc) in the measured sections (Figures 4C and 5C) and structural interpretation (Figures 4B and 5B). For example, at 6 m (20 ft) in Section 1 (designated with an A in Figure 4C and colored yellow in digital version) there is a distinctive bed, about 25 cm (10 in) thick, that consists of current-rippled sandstone (base of Figure 7). This ripple bed is overlain by mudstones followed by a flat-stratified sandstone, which is overlain by about 10 cm (4 in) of deformed sandstone, and mudstone (Figures 4C and 7). These distinctive beds, along with others (e.g. bed B) below, could be identified and correlated throughout most of the outcrop face, as illustrated in Figure 4, although it was more difficult to find these beds in the distal fault set because of poorer exposure of the pre-growth section (Figure 5). The correlations and interpretations were used as the basis to constrain the structural geometry and models for restoration of each major fault.

STRATIGRAPHY AND FACIES

Across the outcrop the distinctive pre, growth, and post-growth strata were described (Figures 4 and 5). The pre-growth section is a mud-rich heterolithic section interpreted as delta front mudstones and sandstones, which contrasts with the growth section of nearly homogeneous interbedded bars and delta front sandstones and shallow distributary channels and bars that are expanded across the faults. A transgressive flooding surface separates the growth section from the overlying strata of Ferron stratigraphic cycle 2 (Gardner, 1995).

At the broadest mapped scale, the delta front sandstones form an upward coarsening facies succession (Figures 4C and 5C) suggesting progradation. Bayward-dipping sandstones in the unfaulted correlative growth succession at the SE end of the outcrop, as shown in an oblique photo (Figure 8), are interpreted as foreset strata associated with the prograding delta lobe. The thickness of the upwards coarsening succession (Figure 9) and height of the clinoform beds approximates water depth, and suggests the pre-growth strata were deposited in a maximum of about 25 m (80 ft) water depth. The homogenous growth sands lie at the top of the growth section, following infilling of this space, and were thus likely deposited in less than a few meters water depth. The stratigraphy and facies are described and interpreted in detail below.

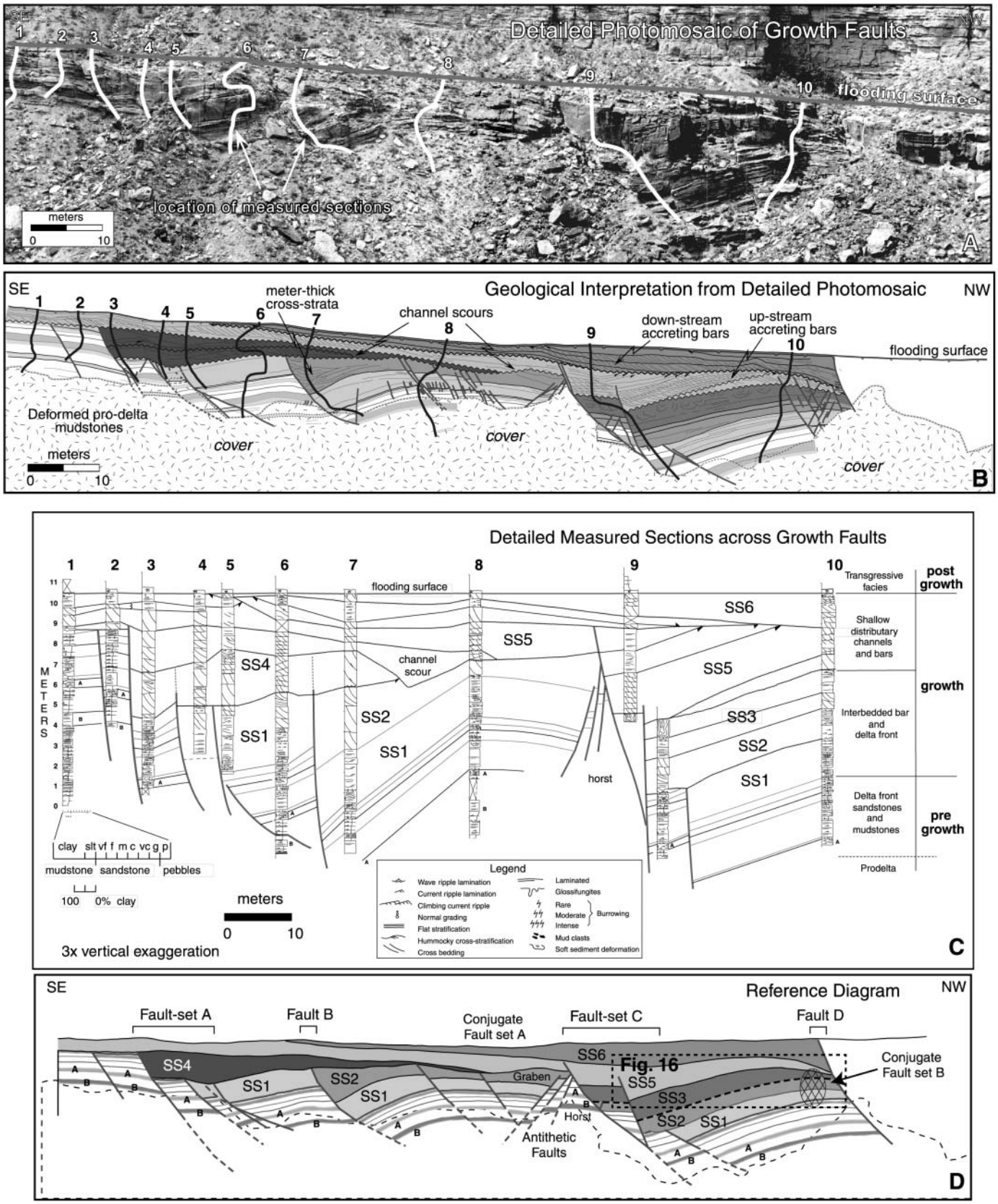

Figure 4. Cross section and interpretation of proximal exposure of growth faults along Muddy Creek showing: (A) detailed photomosaic, (B) geological interpretation of structure, (C) detailed measured sections, and (D) reference diagram. Lettered beds A and B (colored in digital version) are matched to the sands in the measured section and show offset on faults. The growth interval consists of upstream and downstream accreting cross-bedded sandstones deposited in shallow distributary channels and proximal distributary mouth bars. The relative ages of these sands are indicated with numbers SS1 to SS6 from oldest to youngest, respectively. Location of panel shown in Figure 2.

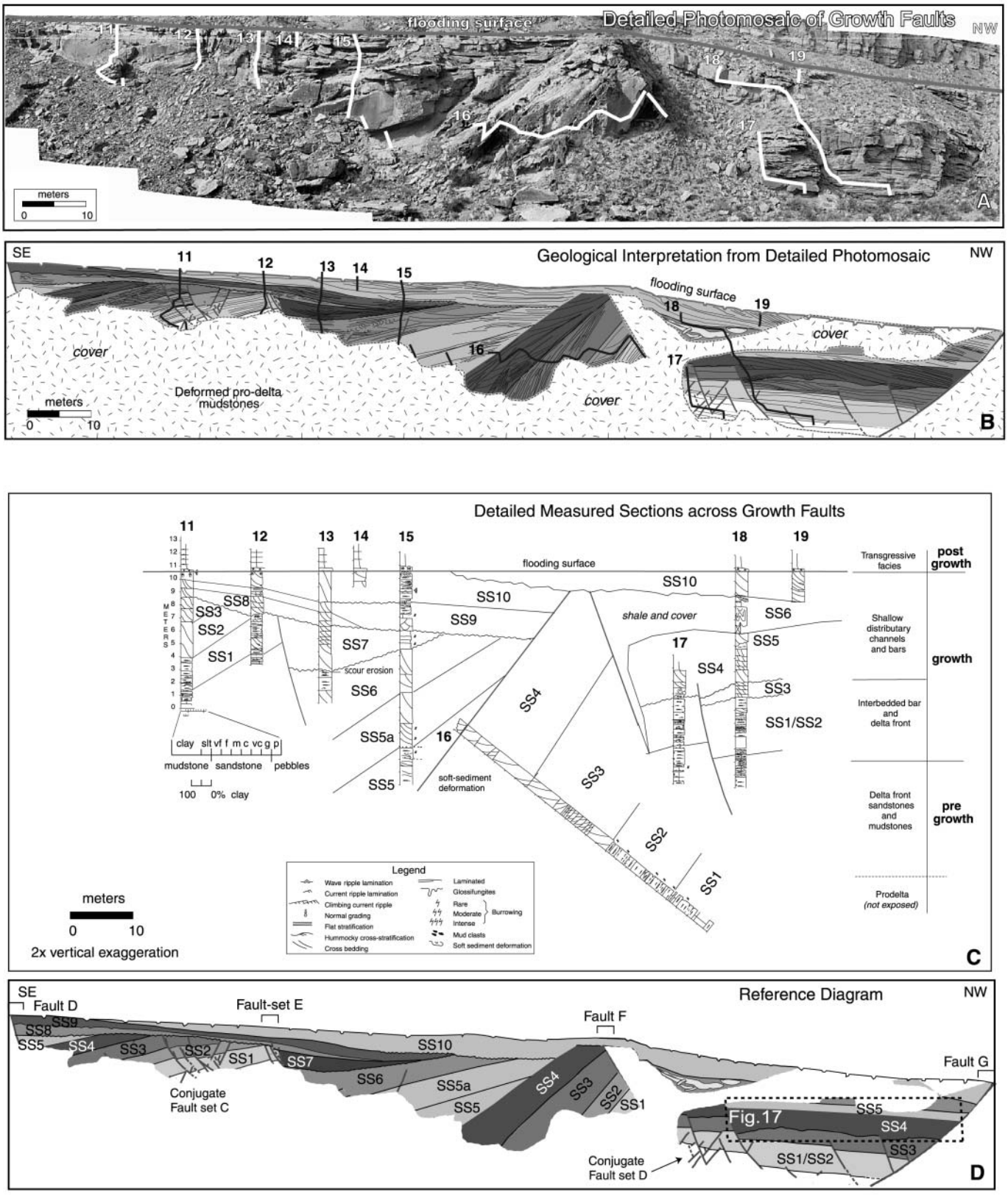

Figure 5. Cross section and interpretation of distal exposure of growth faults along Muddy Creek showing: (A) detailed photomosaic, (B) geological interpretation of structure, (C) detailed measured sections, and (D) reference diagram. Shaded beds (colored in digital version) are matched to the sands in the measured section and show offset on faults. The growth interval consists of upstream and downstream accreting cross-bedded sandstones deposited in shallow distributary channels and proximal distributary mouth bars and larger-scale cross-stratified sandstones interpreted as distal-mouth bar foreset beds. The relative ages of these sands are indicated with numbers SS6 to SS10 from oldest to youngest, respectively. Location of panel shown in Figure 2.

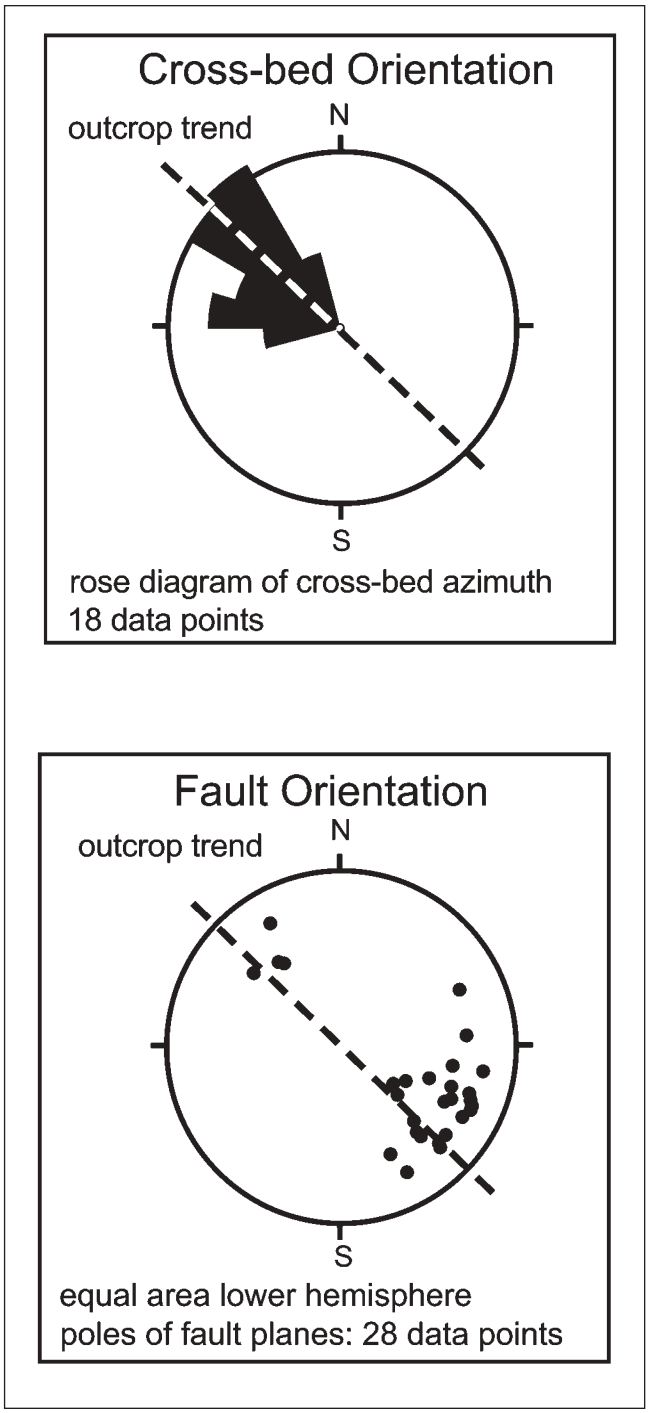

Figure 6. Stereonets of paleocurrents and poles to the planes of faults show that the Ferron delta lobe prograded to the northwest, parallel to the cliff face, and that the exposure is nearly perpendicular to the fault strike which affords a nearly perfect dip view.

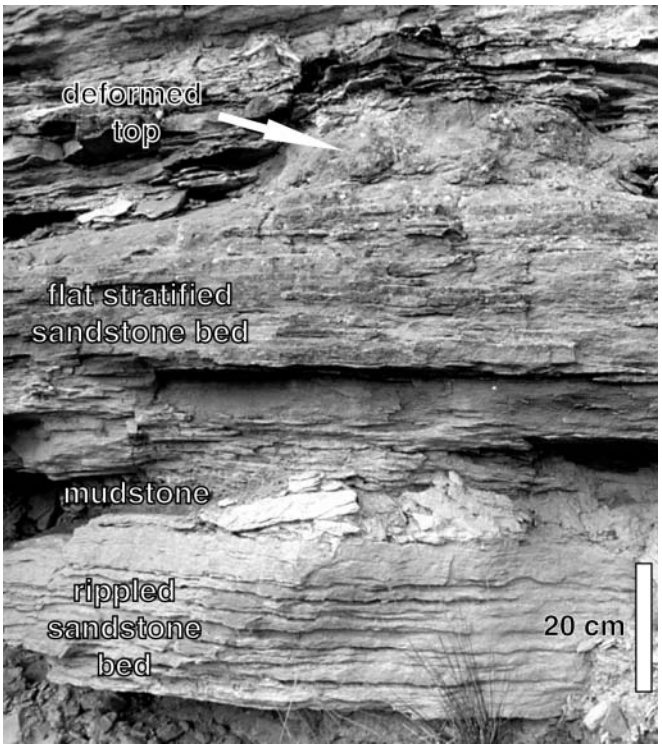

Figure 7. Photograph of key marker beds within the pre-growth section that were correlated across growth faults (see Figure 4). Lower bed consists of ripple-cross laminated sandstones followed by mudstones. Overlying sandstone consists of flat-stratified and deformed strata.

Figure 8. Oblique view of top-truncated, inclined delta front sandstones at southeast end of outcrop.

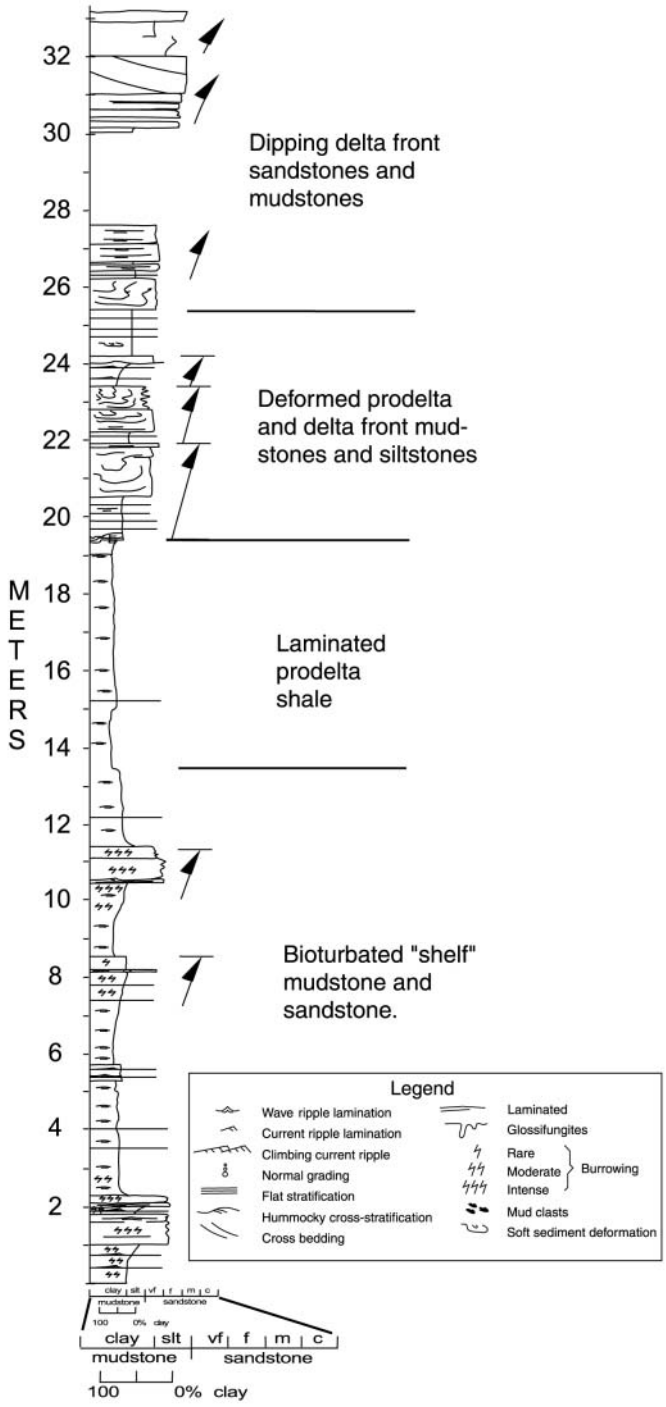

Figure 9. Regional vertical succession measured at southeast end of south cliff along Muddy Creek. Bioturbated mudstone and sandstones, below 13 m (39 ft) are interpreted as being deposited on an open marine shelf. Laminated un-bioturbated mudstones, above 13 m (39 ft), reflect increasing fluvial influence and formation of the Sanpete Valley embayment. Thick zones of deformed strata reflect instability of rapidly deposited prodelta and delta front sediments. The transgressive surface is at 32 m (96 ft). Thickness of the section above the bioturbated shelf facies suggests that the maximum water depth of the bay into which the delta prograded was about 25 m (75 ft).

Pre-Growth Strata

Description

Pre-growth strata are sandstones interbedded with shales in Figures 4 and 5 (colored green, red and yellow in the digital version). The faults sole into the underlying facies, which are covered by rubble within the mapped outcrop, but are well exposed along the cliffs about 300 m (980 ft) to the south in a landward direction (Figure 9). There, the section consists of about 6 m (20 ft) of laminated silty mudstones with rare, very-fine grained current-ripple cross-laminated sandstone beds and ironstone nodules (Figure 10). This passes up into about 7 m (23 ft) of deformed interbedded mudstones and sandstones showing interstratal recumbent folding and loading (Figure 11). This deformed facies passes into interbedded decimeter-thick sandstones and mudstones (Figure 12). Sandstone beds are sharp-based, normally graded and show Bouma-like sequences passing from massive to horizontally stratified and capped by climbing current-ripple cross-lamination (Figure 13). Burrows are few but *Planolites, Skolithos*, and *Arenicolites* occur throughout the succession (Figures 12, 13, and 14) with rare small diameter (< 0.5 cm) *Thallasinoides, Ophiomorpha,* and *Rosselia*. Coalified plant debris is common on parting planes and rare larger woody clasts are bored by marine *Teredolites* (Figure 15).

Figure 10. Laminated mudstones of the pre-growth section. Note lack of burrows and numerous current-rippled sandstone inter-beds. Lack of burrowing reflects fluvial influence and rapid deposition of prodelta sediments. Photo taken at about 20 m (60 ft) in Figure 9.

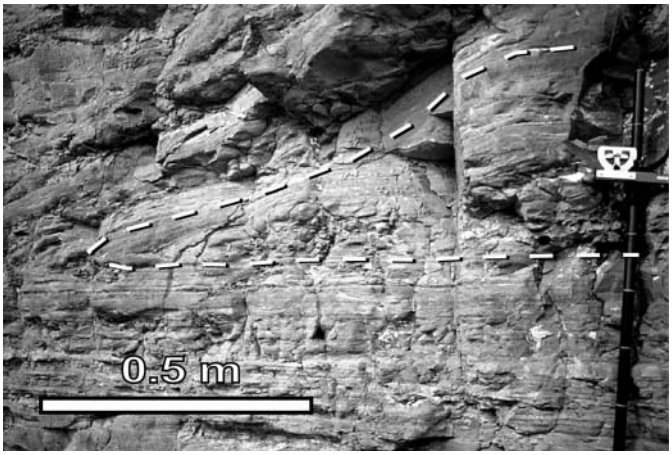

Figure 11. Recumbent fold in interbedded sandstones and mudstones of the distal delta front. Photo taken from strata shown at 22 m (66 ft) in Figure 8.

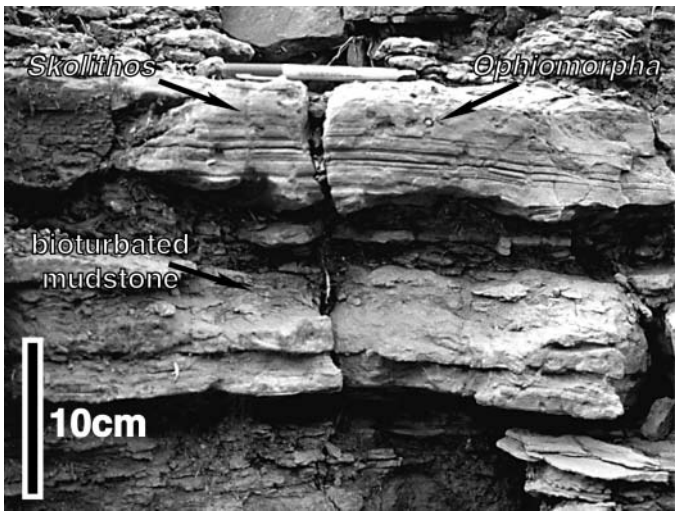

Figure 12. Sharp-based, flat-stratified sandstones with burrowed tops, interbedded with burrowed mudstones.

Figure 13. Photo of graded, flat-stratified, to current rippled sandstones, with thin mudstone interbeds. These are interpreted to form as delta-front turbidites in the pre-growth strata and reflect fluvial dominance.

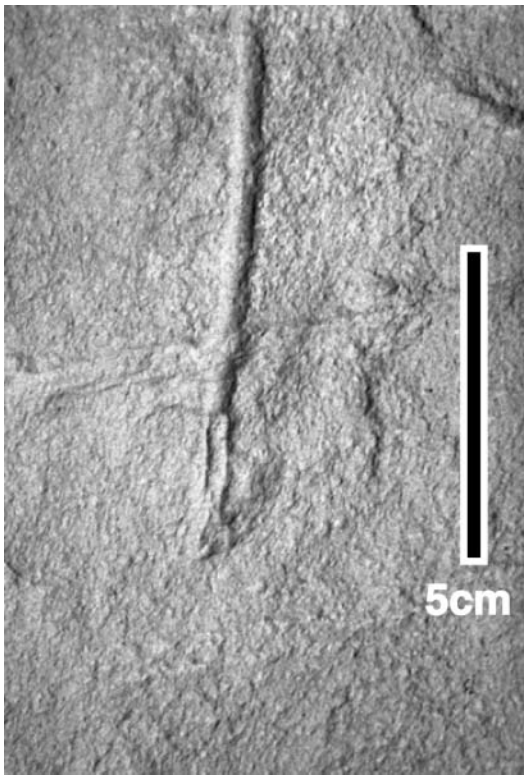

Figure 14. Skolithos trace fossil within stratified sandstones.

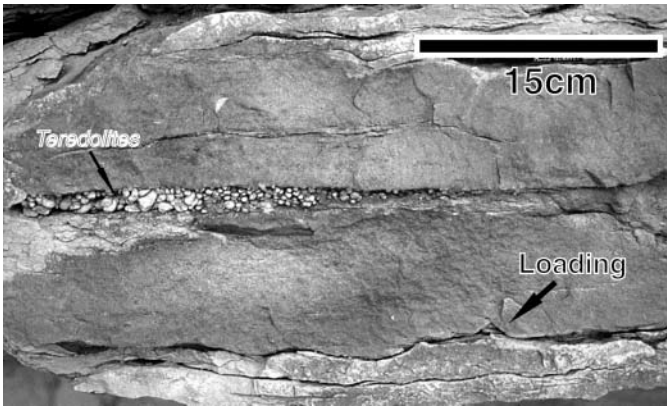

Figure 15. Teredolites bored log forms "grapelike" bubbly looking unit at the base of upper sandstone bed. Coaly material surrounds the casts of the burrows. Sandstones are structureless to flat-laminated to current rippled. Note flame-structures and load casts at the base of the lower sandstone bed.

Interpretation

The low diversity, low abundance, and small diameter of trace fossils suggests a stressed and probably brackish-water environment that was likely proximal to a river mouth (Moslow and Pemberton, 1988; Bhattacharya and Walker, 1992; Gingras et al., 1998). The climbing ripples, lack of burrowing, and abundant load casts and soft-sediment deformation suggest high sedimentation rates that are typical of deposition in a river-dominated prodelta environment (Moslow and

Pemberton, 1988; Bhattacharya and Walker, 1992; Gingras et al., 1998). The loading indicates that the prodelta muds were less dense than overlying more-dense sandstones. Density differences result from the fact that rapidly deposited muds typically have much higher porosity than overlying sands (Rider, 1978). The folding in the muds is interpreted to indicate flow of the early-deposited mudstones and we hypothesize that this basal layer accommodated the displacement at the base of the faults cutting the younger section, consistent with the interpretation of Nix (1999) and Morris and Nix (2000). Dewatering features, such as pipes and flame-structures associated with small-scale loading (Figure 15), indicate that the prodelta sediments were water-logged at the time of deformation and had not experienced significant compaction.

Growth Strata

Description

The growth section forms as a series of 10 offlapping sandstone wedges, labeled SS1-SS10 from oldest to youngest, respectively, in Figures 4 and 5. These wedges consist mostly of fine- to medium-grained cross-bedded sandstones, 2-9 m (7-30 ft) thick, with meter-scale truncation and erosion between cross sets. Paleocurrent directions are strongly unimodal and indicate flow to the northwest (Figure 6). Cross-bedding is also locally organized into climbing co-sets (e.g. between sections 9 and 10, Figure 4 and expanded version in Figure 16). Locally, within individual fault blocks, cross-sets decrease in thickness from 2 m (7 ft) to a few decimeters away from the faults (Figure 16).

At the scale of the entire exposure, the offlapping organization of the growth sands also shows that cross-sets step seaward. In the most distal portion of SS4 (Figures 5, 17) similar medium-scale cross beds pass seaward into a single thick set of inclined strata. These thick single cross-stratified sandstones have a distinctly sigmoidal shape (Figure 18). Much less mudstone was observed in the growth section compared to the pre-growth section, although the sigmoidal cross-stratified sandstones can ultimately be traced into heterolithic facies in more distal exposures of the delta lobe. As an example, SS1 sandstone at the base of measured sections 4 and 5, in Figure 4C correlate with the more heterolithic strata of SS1 in measured section 10 at the base of the growth section.

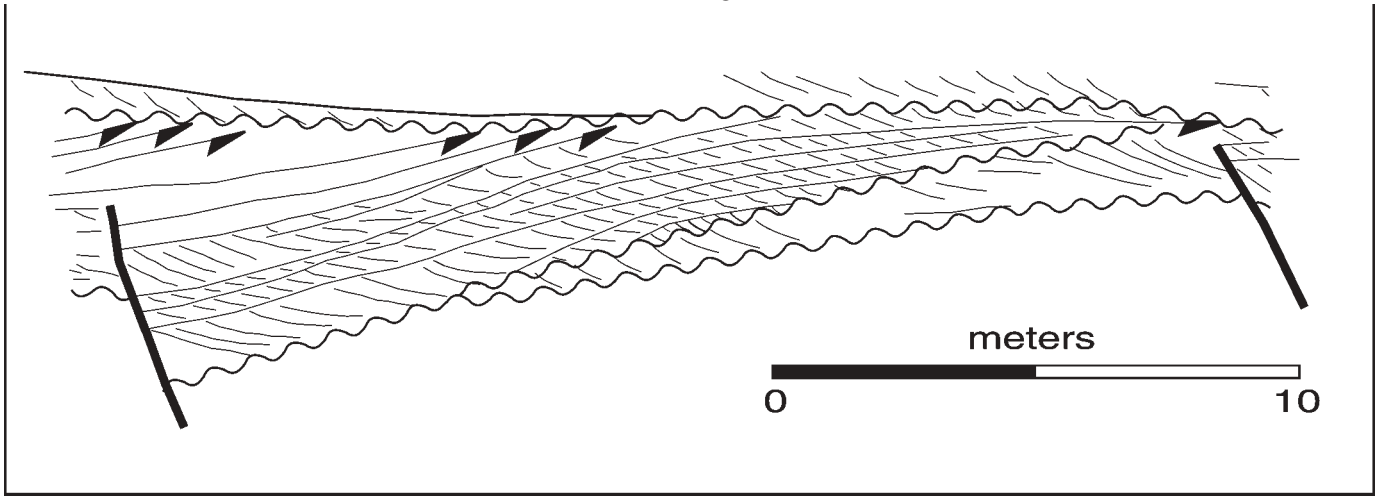

Figure 16. Upstream accreting cross-strata interpreted to form on the inner margin of a distributary-mouth bar. Closeup of bedding diagram of SS5, between measured sections 9 and 10 in Figure 4B.

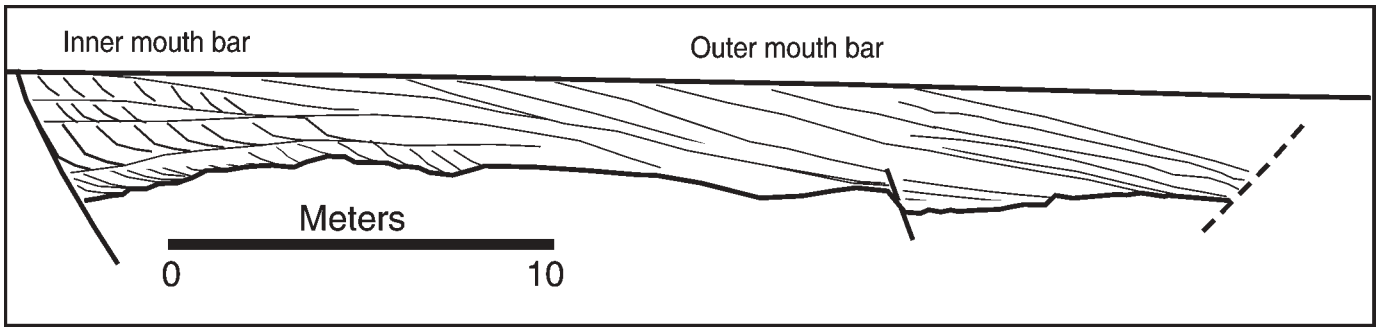

Figure 17. Bedding diagram showing dune-scale cross-strata, formed in the inner-mouth bar, passing into outer mouth-bar foreset strata. Detail is of SS4, immediately northwest of measured section 18 in Figure 5B.

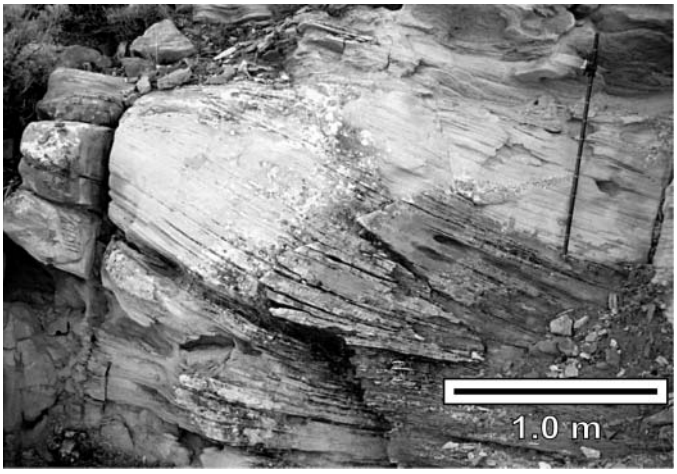

Figure 18. Large-scale sigmoidal cross-strata, interpreted to form as foresets on the prograding distal, outer-mouth bar.

In places, the larger scale sigmoidal strata are draped by mudstones, as seen in SS10 at 1 m in section 19 (Figure 5C). These cross-stratal units also locally show 2-3 meter-thick (6-9 ft) upward coarsening successions. In places a gradational contact with underlying mudstones is seen (e.g. section 15 in Figure 19). Locally the large-scale cross-strata pass from massive medium-grained sandstones, such as from 8-9 m (24-36 ft) in section 13 (Figure 19) bayward into finer-grained ripple cross-laminated sandstones interbedded with thin muds (section 15, Figure 19). The ripple cross-laminations are organized into spectacular near-vertical climbing sets (Figure 20) suggesting very high sediment aggradation. Some of the ripples look symmetrical in plan view indicating some wave-activity during deposition.

Locally growth sandstones also show extensive soft-sediment deformation and dewatering structures, such

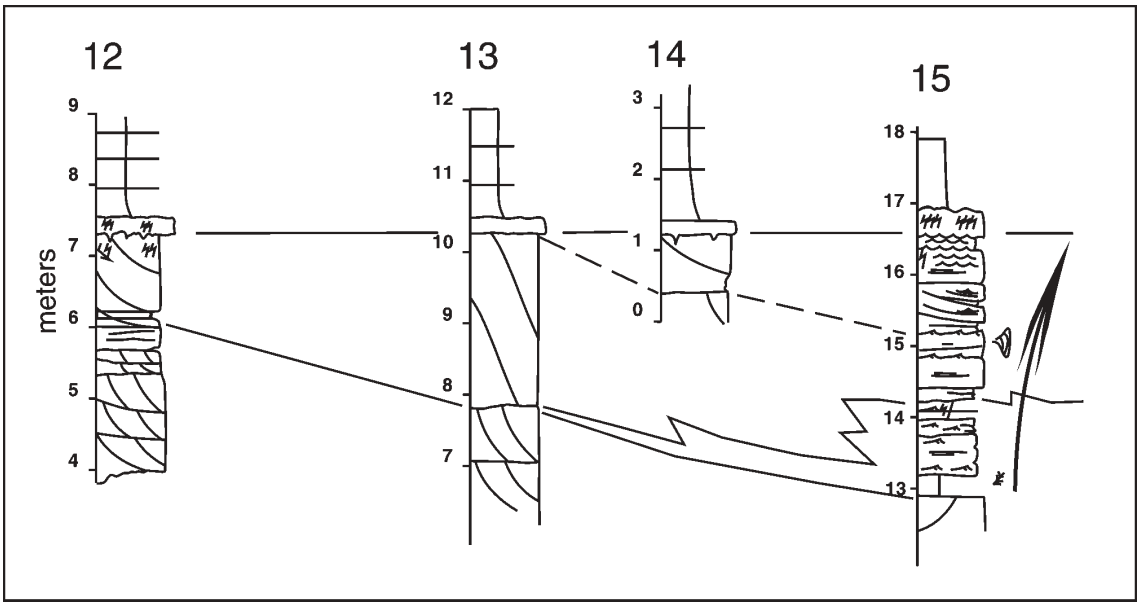

Figure 19. Closeup of SS11 in sections 12-14 (Figure 5) showing passage from sandstone into muddier strata. Two-m (6-ft) thick sets of inclined strata form as foresets on the prograding distal margin of a mouth bar. Distal deposits in section 15 show near-vertical climbing ripples and display a coarsening-upward facies succession.

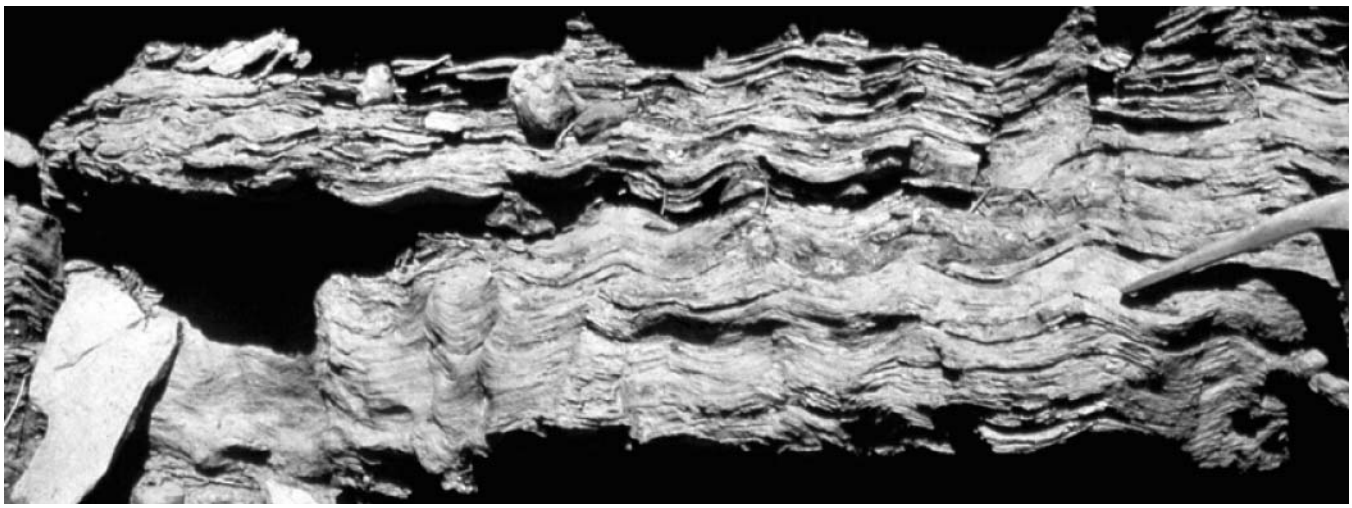

Figure 20. Vertically climbing symmetrical ripples formed in a distal-mouth bar. Note edge of the rock hammer for scale at right side of photo.

as dish structures and pipes (see sandstone SS3, between sections 9 and 10, Figure 4C).

Interpretation

The medium-scale cross-strata represent shallow-water, migrating subaqeous dunes. The truncation associated with the dunes suggests that they formed within shallow (a few meters deep) distributary channels in the proximal delta front (channel scours are labeled in Figures 4B and C). Decreased preservation of cross-strata within the hanging walls suggests that the faults were moving during deposition of the cross-bedded sands. The climbing cross-sets possibly indicate high sand aggradation rates and upstream accretion of bars. Alternatively, cross-sets might step landward as rotation on the hanging wall increases towards the fault. The landward-stepping and seaward-stepping cross-strata show that both upstream and downstream accretion of sands has occurred, as is seen in modern river-dominated deltas (Van Heerden and Roberts, 1988). The organization of cross-strata suggests that fault movement and sand deposition were roughly synchronous and reflects an intimate interplay between sedimentation and the formation of faults.

The larger sigmoidal features are interpreted as the topset, foreset and bottomsets of prograding distributary-mouth bars, rather than the smaller-scale dune bedforms within distributary channels (Figures 18, 3B). The thickness of the mouth bars likely approximates water depth and suggests depths of a few meters. The smaller-scale cross-strata are interpreted to lie at the inner margin of the delta front within the region confined by the most distal, "terminal" distributary channels (Figure 3). The large-scale sigmoidal cross-strata represent the region of unconfined flow at the bayward (distal) margin of a distributary-mouth bar and can be identified throughout the cross sections (Figures 4, 5).

In the distal fault exposure (Figure 5), units SS8 to SS10 contain a greater proportion of prodelta mud and prograde over a complex topography caused by foundering of the underlying growth strata. This mud may have been injected along Fault E, but there is also evidence that prodelta muds were deposited along with sandstones SS8-SS10. This style of deformation and sedimentation is somewhat more similar to the style of synsedimentary faulting described by Nemec et al. (1988) and by Pulham (1993) in which failure of the delta front and proximal slope occurs first forming a complex seafloor topography that is then later infilled or "healed" with prodelta and delta front sediments.

The thickness of these younger offlapping, upward-coarsening facies successions, also likely approximates water depth, and suggest the submarine topography was only on the scale of a few meters to 10 m (30 ft) deep. The soft-sediment deformation and estimation of water depths from facies shows that all of the growth faulting occurred in less than about 10 m (30 ft) water depth, while sediments were still waterlogged and before significant compaction had occurred.

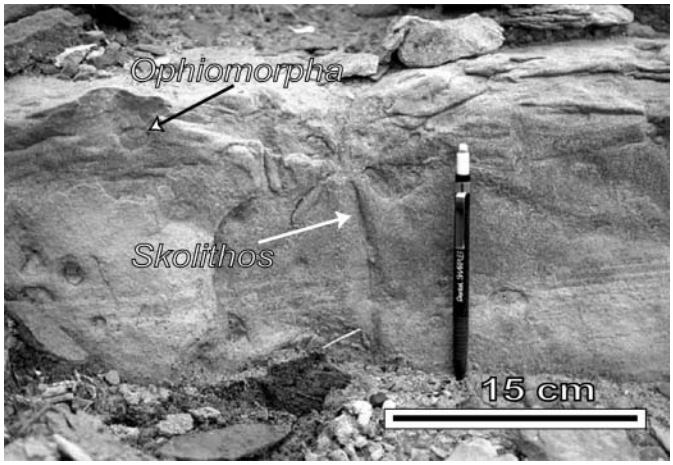

Figure 21. Bioturbated coarse sandstone with Skolithos and Ophiomorpha burrows, overlying cross-stratified sandstones. This facies is interpreted to mark the transgressive lag across the top of the drowned delta lobe and can be traced across the top of the cliff.

Post-Growth Strata

The overall growth succession is truncated by a decimeter-thick bed of bioturbated sandstone containing abundant centimeter-diameter *Ophiomorpha* and *Skolithos* burrows (Figures 4, 5, and 21). This bed is in turn overlain by marine shales at the base of the next upward-coarsening succession in stratigraphic cycle 2 of Gardner (1995). No mapped faults persist above this bioturbated unit showing that growth faulting ceased with the transgression of the lobe and deposition of this thin sandstone.

STRUCTURE

The predominant structural style across the entire mapped outcrop is seaward (northwest) dipping listric normal faults with extensive growth of the strata into the hanging wall of the faults. The faults curve gently along their length as dip decreases and terminate in a mud-rich prodelta section underlying the prograding sands. The upper tips of the faults terminate near or below the overlying flooding surface that separates the faulted growth section from the unfaulted overlying strata of Ferron stratigraphic cycle 2. The upper portions of the faults dip at an angle of approximately 70°. The basal fault terminations are covered, however, preventing a complete description of their lower geometry.

A set of regularly spaced individual faults and fault sets separate the growth sections along the exposure. These are labeled as Fault or Fault-set A to F in Figures 4

and 5. A fault-set is two or more closely spaced faults that together bound an extended growth section in their composite hanging wall.

From southeast to northwest, or from a landward to bayward direction, the facies architecture shows a thickening of the nearly homogeneous cross-bedded sandstones across the outcrop. Clearly, the thickening is structurally controlled with dramatic changes across the faults, but the thinner more proximal growth section (Figure 4) exposes the underlying heterolithic pre-growth section, which is nearly completely covered in the distal location. The unique facies within the pre-growth section are more easily correlated and restored across the faults in the thinner proximal mapped exposure (Figure 4) than in the thick cross-stratified sands that comprise nearly the entire distal mapped exposure (Figure 5).

Proximal Exposure

The proximal exposure is divided into three major fault blocks separated by Fault-set A, Fault B, and Fault-set C (Figure 4D). The pre-growth section is exposed well enough across the proximal exposure to measure the throw across the faults. The composite throw, totaled across all of the faults in the proximal exposure, is approximately 13 m (40 ft), although the throw across any individual fault is at most a few meters. This section is folded as it is displaced along the curved growth faults. The shallowest prograding sandstones overlying the strongly folded section are less strongly deformed and they show a distinct, offlapping, prograding stratal geometry. The pre-growth section, as described above, is a heterolithic section of thinly bedded sand and shales (Figures10 through 13). The growth section is a nearly homogeneous section of cross-bedded sandstones. Shales occur in the growth section only locally as discussed above.

Fault-Set A

The first major growth section in a landward direction in the proximal exposure is bound by a set of three faults (Fault-set A) across a zone 10 m (30 ft) wide. The faults step down into the section from a proximal to distal position. The most proximal and shallowest fault in the set offsets a wedge of cross-bedded sandstone (SS4) that is thickest against the fault and thins in a bayward position, pinching-out landward of Fault-set C (Figure 4). The upper fault tip terminates at the bed surface separating SS4 from the overlying prograding sand (SS5) that thickens across Fault-set C in a more distal location. The gentle curvature of the underlying bedding surface suggests that the deeper section rode passively with the stratigraphic growth against this fault.

The other two more distal faults in Fault-set A are older faults with a shallower dip than the proximal fault in the set indicating that they have also rotated with stratigraphic growth and displacement across the youngest fault in the set. This fault pair terminates at the bed surface between SS1 and SS4. Although there is large differential offset across these faults deeper in the section, the mapped displacement across the base of SS1 shallow in the section is small across the more distal fault in the set. The two distal segments in Fault-set A most likely represent the overlapping tip regions of two contemporaneous faults forming a transfer zone or relay ramp (Peacock and Sanderson, 1991, 1994) across which throw is transferred. The measured throw across Fault-set A in the pre-growth section is 8 m (24 ft).

Fault B

A single fault (Fault B) cuts the section approximately 15 m (45 ft) seaward from the outermost fault in Fault-set A (Figure 4). The fault is strongly curved along its length, which is consistent with the strong curvature of the beds in the hanging wall. Fault B terminates against the base of SS4 like the set of faults in the hanging wall of Fault-set A, but cuts a thicker cross-bedded sand growth section than the previous set. The cross-bedded sand (SS2) comprises the growth fill in the hanging wall of Fault B.

In the distal hanging wall of Fault B (the proximal footwall of Fault-set C) is a set of conjugate faults (Conjugate Fault-set A; Figure 4) bounding a graben. These faults most likely formed in response to the bending of the layers (McClay, and Ellis, 1987; McClay and Scott, 1991; Brewer and Groshong, 1993). The beds thicken into the hanging wall of the antithetic faults dipping to the southeast and bounding the graben to the northwest. These antithetic faults, together with the synthetic faults in Fault-set C, bound a complementary horst to the graben (Figure 4D). The thickening of the section across the antithetic faults suggests that they were active at the same time as Fault B. The synthetic faults in the conjugate fault set are more numerous than the antithetic faults and comprise tens of closely spaced faults with lengths from several centimeters up to 10 m (30 ft) and throws of millimeters to 30 cm (12 in) (Figure 4B).

Fault-Set C

Fault-set C is the most distal fault set in the proximal exposure and comprises three faults that step down into the section from a proximal to distal location as in Fault-set A. The most proximal fault in the set beheads the antithetic faults bounding the graben. The shallow prograding sand, SS5, expands across this fault, which terminates at the base of the youngest prograding sand in the proximal exposure, SS6. The central fault in the set connects along the deeper trace of the proximal fault in

the set. The most distal fault in the set terminates at the upper bed surface of SS1 similar to the deep faults in Fault-set A.

The distal hanging wall of Fault-set C has a set of conjugate faults, which we also interpret as related to bending (Conjugate Fault-set B, Figure 4D). In this case, however, the lateral extent of the faults in the set is narrow and the conjugate fault pairs are nested up through the section with no growth across the faults.

Distal Exposure

The distal mapped exposure (Figure 5) is markedly different from the proximal exposure (Figure 4) in several important ways. The pre-growth section is nearly completely covered with only the thick cross-bedded growth section exposed. This limits the accuracy of the fault restoration and estimates of throw. In addition, most of the major growth faults are covered with only local exposure of the fault tips. We infer the presence of the faults by the dip of the beds, but the poor exposure prevents as detailed an interpretation as in the more proximal exposure. The bed dip increases across the entire mapped outcrop and dips are greatest in this distal exposure.

Fault D

The first or most proximal fault in the interpreted section in Figure 5 is labeled Fault D. This is the fault at the distal end of the hanging wall in Fault-set C (Figure 4). Only the upper 5 m (15 ft) of the fault is exposed and although mapped as a single fault at the scale of the map, in detail it is a narrow zone approximately 1-2 m (3-6 ft) wide of thin fault segments and deformed sand. Massive shallow beds of growth strata (SS8 and SS9) immediately adjacent to the fault in the hanging wall are only slightly rotated towards the fault and form large-scale cross-bedded sandstones that thin seaward. These young prograding sands dip gently bayward in their more distal position. Their offlapping stratal geometry is similar to the younger prograding sands (SS5 and SS6) in the proximal section, but correlation across the fault is difficult.

Beneath the gently dipping prograding sands, SS8 and SS9, is a thick section of nearly uniformly thick cross-bedded sands (SS1 to SS5). The beds are rotated and truncated by an erosional surface across which lies the prograding section. The facies of the rotated beds is indicative of the growth sections, but their down-dip termination towards fault D is covered. Near the very base of the section about 1 m (3 ft) of interbedded shales and sandstone is exposed (sections 11 and 12, Figure 5C), which we correlate with the pre-growth section described earlier.

Although the section is incomplete because of erosion and cover, the exposed beds have a nearly uniform thickness of approximately 10 m (30 ft). This thickness is equivalent to the growth section close to the faults comprising Fault-set C and we interpret these as the same beds (SS1 to SS5).

A conjugate set of faults (Conjugate Fault-set C, Figure 5D) cut these thick beds in a distal location of the hanging wall of Fault D just below the erosional surface. The conjugate fault pairs in the set form a 10-m-wide (30-ft) graben that narrows deeper in the section to the intersection of the fault pairs. The lower terminations of the outer faults bounding the graben are covered. These conjugate faults most likely formed in response to the bending of the layers (McClay, and Ellis, 1987; McClay and Scott, 1991; Brewer and Groshong, 1993).

Fault-Set E

At the distal ends of the thick dipping cross-bedded sands in the hanging wall of Fault D are a set of faults, which are exposed only along their upper extent (Fault-set E, Figure 5). This set of faults extends horizontally over a zone approximately 2 m (6 ft) wide. We interpret these faults to be the upper terminations of a listric growth fault set bounding the next bayward section of thick cross-bedded dipping sands. Between Fault-set E and Fault F is the thickest growth section exposed in the outcrop. The rotated beds in the most distal part of the hanging wall of Fault-set E have dips up to 45° southeast. This strongly rotated fault block acts as a buttress to the overlying prograding sediments.

Because the faults bounding this growth section are covered, we are uncertain of the deeper fault geometry. It is likely, based on the structural style in the proximal section and on our restorations, that this extensive growth section developed across several sub-parallel listric faults.

The shallowest growth section completely truncated by Fault-set E, SS7, thickens on the downthrown side of the exposed fault trace and thins onto the dipping hanging wall over a distance of approximately 10 m (30 ft). Onlap of individual sigmoidal cross-strata against the fault, suggest that a distributary-mouth bar prograded into the actively growing space. The base of the prograding sands overlying this wedged section is slightly offset by the fault. The youngest prograding sands overlying this section (SS9 and SS10) are thickened over the hanging wall, but are not faulted indicating some differential compaction in the hanging wall of the fault.

Beneath this youngest section of prograding sands, the cross-bedded sands in the hanging wall of Fault-set E maintain a nearly uniform thickness across their length. This implies that the sands were deposited over a broad surface that was not strongly dipping, which is very different from the youngest sands with a prominent wedge shape.

The thick steeply dipping cross-bedded sands that terminate against Fault F at the distal end of the hanging wall in Fault-set E are the oldest growth section in this fault block. A heterolithic section exposed at the base of the sands (Figure 5C; section 16) we interpret as pre-growth. We therefore, correlate the thick steeply dipping sands, which overlie the pre-growth section with SS1 to SS4 exposed in the hanging wall of Fault D and Fault-set C. The trailing edge of these sands in the hanging wall of Fault-set E are sharply truncated by Fault F, which is a distinct planar surface in outcrop.

The thick sand beds above the SS1 to SS4 section are slightly discordant with the underlying section. The older beds in the section (SS5), onlap the upper bed surface of section SS4, but without lateral thinning of individual beds in the section. The upper most beds in the thick section are truncated across their thickness by an erosional surface separating the older dipping section from the younger prograding sands SS9 and SS10.

We interpret the bedding surface separating SS4 from the overlying discordant beds of SS5 as a bed-parallel fault. Slip on the fault would account for the onlapping relationships. The youngest prograding sands, SS10, thicken across the southeast dipping beds of SS4 lending credence to the interpretation that this bed surface acts as a fault displacing the beds antithetic to the primary growth orientation along the bayward dipping faults.

Fault F

The most distal mapped section in the outcrop is a flat lying section of heterolithic sands and shales overlain by cross-bedded sands with an anomalous, shale section near the top. This section is unique in the outcrop because the beds are not rotated across Fault F as in the style observed in other bayward dipping faults. The style of unrotated beds suggests that Fault F is not a curved listric fault, but is planar. As we show in the section on fault restoration, we interpret this as a fault rotated from a southeast dip to a northwest dip.

The correlation across this distal exposure to the other mapped sections is difficult because of erosional unconformities through the section. We associate the heterolithic beds at the base of the section with the heterolithics at the base of the steeply dipping beds in the footwall of Fault F. The cross-bedded sands above these heterolithics are thinner than the cross-bedded sands comprising the hanging wall of Fault-set E.

Above the cross-bedded sands capped by SS5 in the flat lying section is a shale-rich section 3-5 m (9-15 ft) thick. This shale is anomalous in the younger growth section, which is mostly homogeneous cross-bedded sandstones across the outcrop. The total thickness of the shale in this fault block is uncertain because much of the area is covered. Adjacent to Fault F, however, a thin exposed sand layer is folded and contorted within the shale section. The deformation of these sands most likely formed due to gravity collapse with progradation across the buttressed high of the rotated distal footwall of Fault E onto the steep dip of Fault F.

The anomalous shale shallow in the clastic section may have been injected along the fault plane of Fault F or be the distal muddy influx from a prograding sand. Nix (1999) and Morris and Nix (2000) hypothesize that the shale is diapiric and sourced from the underlying prodelta muds. One possible mechanism for the emplacement of muds shallow in the section from a deeper source is overpressure of the muds and injection along the fault plane. The steeply dipping rotated beds truncated by Fault F lie above a regional dip as demarcated by the base of the youngest prograding sand. This sand thickens on either side of the buttressed fault block. The differential relief across the block suggests that the shale beneath the block is fully compacted, unlike the prodelta muds on either side, which compact slowly to accommodate the growth section. The rotation and bayward displacement of this block may have overpressured the muds driving them up the fault plane. Trenching along the fault plane seems to support this hypothesis although it remains inconclusive as to whether the trenched muds are in place.

The alternative explanation for the shallow muds is that they are the distal muds of a prograding sand. This hypothesis may be supported by the evidence of muds in SS9 measured in section 15 (Figure 5C). These muds may have prograded across the rotated beds into the more distal section. Our correlation of the beds across the buttressed block does not agree with this interpretation, but the correlation of beds in this distal location is arguable. The exposures are still too limited to support one hypothesis more strongly over the other.

At the base of this distal section adjacent to Fault F is a set of conjugate faults labeled Conjugate Fault-set D. Although these faults are not in a present-day folded distal hanging wall as the other conjugate fault sets, our restorations show that they are most likely an older set that formed in the curved footwall of the nascent Fault-set E.

The exposed limit of the mapped cliff-face extends approximately 50 m (150 ft) beyond the cross-sections described. Much of this unmapped exposure is covered but at the most distal end is a partly exposed thick section of cross-bedded sands with a small counter-clockwise rotation apparently in response to displacement on a fault covered beneath the rock rubble.

FAULT MECHANISMS

As we have shown in our description, no growth faults extend above the flooding surface separating the growth section from the overlying Ferron stratigraphic

Figure 22. Sand and shale smear within a narrow fault zone separating beds in the heterolithic pre-growth section.

cycles. The facies interpretation suggests that the cross-stratified growth section was never deposited in water more than a few meters deep. These observations and the obvious growth of the section across active faults is proof that the faults nucleated and remained active during only shallow burial that scales with the maximum depth to which the faults extend, which we expect to be less than 30 m (90 ft).

The active fault mechanisms at these depths are restricted to deformation in soft-sediments such as shale and sand smear and disaggregation zone mixing or grain-rolling in narrow zones without concomitant grain-crushing (Fisher and Knipe, 1998). In the following discussion we describe some of the detailed fault mechanisms observed in the outcrop.

Shale and Sand Smear

In shallow-marine siliciclastic sediments, shale smear along fault planes is a common mechanism described in surface outcrops (Lindsay et al., 1993) and sub-surface reservoirs (Berg and Avery, 1995; Yielding et al., 1997). Shale smeared along the fault plane from a source layer is commonly interpreted to be a sealing mechanism between hydrocarbon-filled sands juxtaposed across faults in oil and gas reservoirs. Less commonly described is sand smeared concomitantly with the shales along the fault plane. Because of the soft state of the sediments deformed across the growth faults, sand and shale are commonly observed smeared along the planes of faults in the Ferron outcrop.

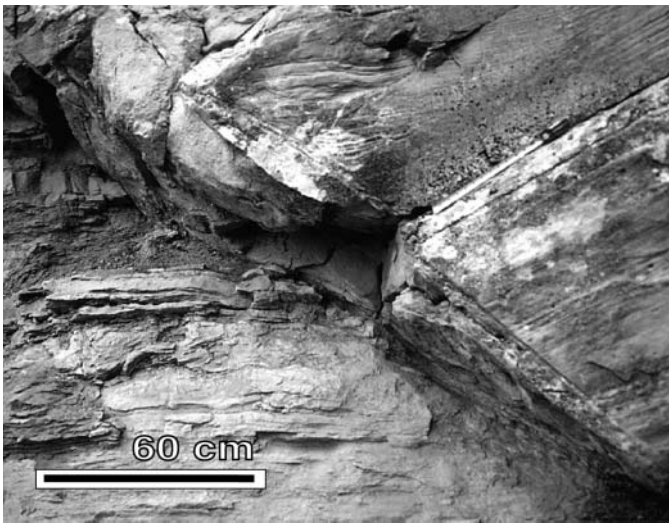

Figure 23. Faulted contact between the cross-bedded sandstones of the growth section on the right and the heterolithic pre-growth section to the left. The fault is a zone of thin seams interpreted to be local disaggregation and mixing of the grains.

Mud-rich fault smear occurs where the faults are exposed cutting the pre-growth section of sands and shales. Figure 22 shows the lowermost section of a fault segment along Fault-set A (Figure 4) showing sand and shale entrained along the fault plane. Although the beds adjacent to the fault would have been unconsolidated during the deformation, the fault forms a narrow zone 5-10 cm (2-4 in) wide. Within this zone, sand and shale beds are attenuated and smeared. In places, sand wedges within the fault zone are shingled. In most cases, the beds within the fault zone are disconnected from their source layer outside the fault.

Disaggregation Zones

Faults that cut the thick homogeneous sections of cross-bedded sands are often manifested in outcrop by a thin trace darker or lighter in color than the host sand. The fault trace in the sands is most likely a narrow zone, millimeters wide, of grains that roll around their grain boundaries to a more tightly packed configuration without grain crushing. This mechanism has been called disaggregation zone mixing (Fisher and Knipe, 1998). Limited micro-structural analysis of these zones confirms this interpretation. The local compaction of the grains within the fault zone reduces the permeability within the fault zone, but not sufficiently to act as a seal between sands juxtaposed across the fault. Petrophysical studies of these rocks show that the faults may seal if developed in host rocks with clay greater than 15% (Fisher and Knipe, 1998).

Figure 23 shows several closely spaced disaggregation faults in a growth section within a zone 5-10 cm (2-

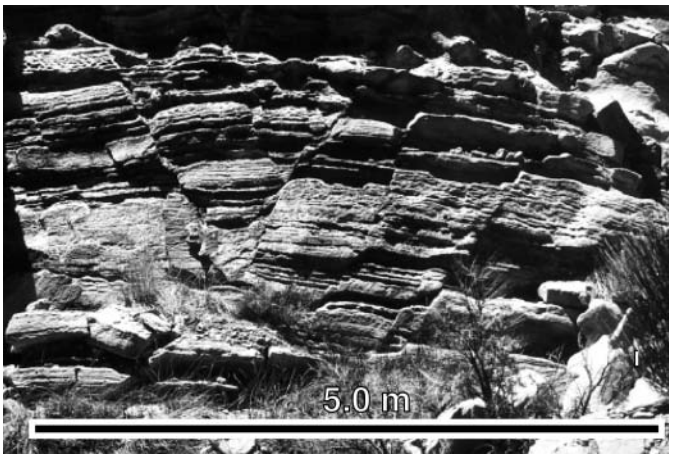

Figure 24. Conjugate fault-set B cutting flat-stratified sands in the hanging wall of Fault-set C.

4 in) wide. The fault zone separates a thick growth section of cross-bedded sands on the right from the heterolithic pre-growth section to the left, in Figure 23. As in the example of sand and shale smear, the beds adjacent to the fault are not deformed. Within a narrow zone adjacent to the heterolithic section sand and shale is smeared along the fault zone. The trace of the disaggregation faults can be followed up the section into the sand on sand contact, but it is more difficult to follow in outcrop.

The thick sand section in the distal hanging wall of Fault-set C is cut by a conjugate fault (Conjugate Fault-set C; Figure 4). These faults formed later in the deformation after bending and with no growth across their boundaries (McClay, and Ellis, 1987; McClay and Scott, 1991; Brewer and Groshong, 1993). The strata in the distal sands are eroded into distinctive bed sets that can be traced across the faults (Figure 24). These faults as in the other examples formed in soft sediments by disaggregation zone processes.

Mixed Mechanisms

Not all of the fault displacement occurs across discrete fault planes or narrow fault traces. In several cases, the displacement is accommodated across closely spaced faults within zones up to 1 m (3 ft) wide. Figure 25A, for example, shows several faults cutting the pre-growth section of thinly bedded sands and shales. The bed offset of 30 m (90 ft) is shared among several closely spaced faults accompanied by a narrow monoclinal bend of the rocks.

In Figure 25B, the displacement is similarly accommodated across several discrete faults in a narrow zone. In this case the deformation style is a conjugate fault set. The faults dipping to the right displaced the section and then they are offset by the fault dipping to the left. Several beds entrained in the left-dipping fault are attenuated during the deformation. Attenuation of the thinner sandstone beds by small local closely spaced faults is a common mechanism in the pre-growth section.

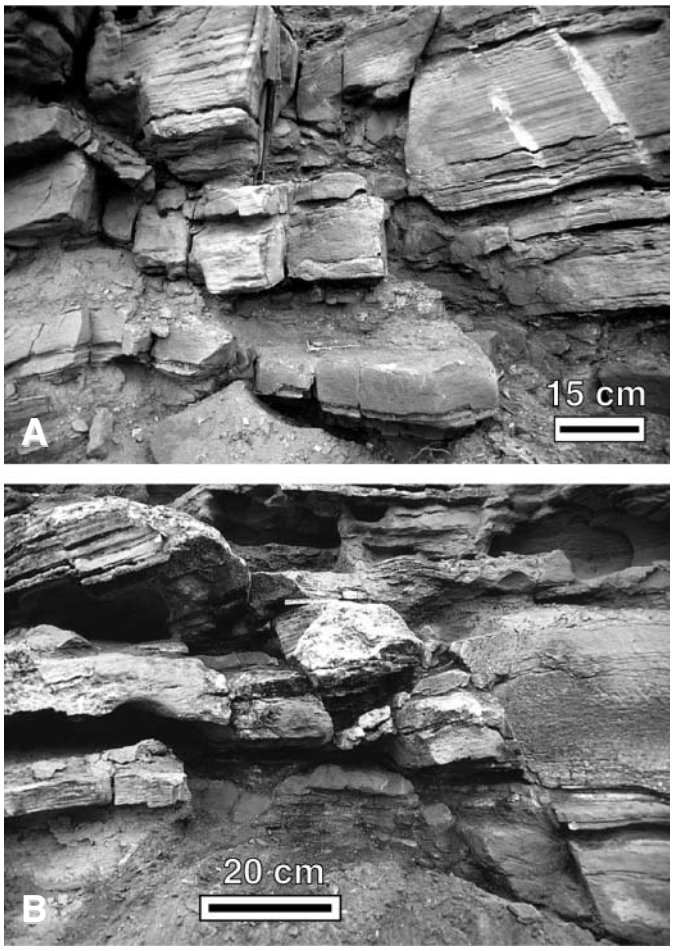

Figure 25. (A) Multiple small displacement faults accommodating a larger composite throw across the zone containing the faults. (B) Multiple faults dipping to the right are offset by a later fault dipping to the left. Both fault sets cut the pre-growth section in the distal hanging wall of Fault B.

STRUCTURAL RESTORATIONS

Many models have been proposed for the restoration or back-stripping of structural cross-sections to validate the interpretation and constrain their historical development. One method described is flattening of sequential stratigraphic horizons (Dula, 1991). In this method, particle paths are required to move vertically, and if the layer is curved in the deformed state the line length is shortened in the restored state. If the bed area is not maintained by thickening of the layer during this restoration, the bed area will be reduced in the restored state. An alternative restoration method is to maintain the line length and bed area during the restoration. Restoring a curved surface in this scenario requires bed slip.

More sophisticated methods for "kinematic" restoration have been proposed that assume *a priori* the particle path based on the bed and fault shape. The section is restored along these particle paths. The assumptions inherent in these techniques must erroneously estimate the "true" particle paths. They do, however, constrain the restoration along a path parallel to the fault that results in reasonable restored surfaces through time and preserves the bed length and area.

We restored both the proximal and distal fault interpretation in this study to investigate the fault timing and constrain the interpretation of the fill style and history. For several reasons we used different restoration techniques for the proximal and distal exposures. In the proximal set of faults, we restored the faults using a kinematic approach. The bed shapes were used to predict the fault shale at depth – curved beds result in curved or listric faults, and the beds were restored to their pre-faulted position along the interpreted faults (Dula, 1991). We used ARCO in-house proprietary software for the restoration.

In the more distal fault set, the faults have a more complex style and bed-fill history. Because of the added complexity and because the software available for the previous study was no longer at our disposal we relied on a restoration of line length and area balance for the interpretation.

The kinematic restoration technique displaces the section along paths parallel to the fault and so we often assume that this method is more rigorous. Although neither of the two methods described for restoration accurately describes the particle motion, both restoration techniques provide us with an interpretation of the fault timing and fill history of the normal faults. A more rigorous interpretation would require knowledge of the material properties and boundary conditions. The sequential restorations as described for the proximal and distal fault sets do not correlate as one-to-one time steps because of the progradation of the section over the outcrop distance. The more proximal fault sets have a greater number of restored steps early in the growth history than the more distal fault sets, which have a greater number of steps in the later fault history. Although these restorations constrain the timing of the faults, the difficulty in correlating a proximal growth sand with a distal sand introduces uncertainty into the analysis. The uncertainty is discussed where appropriate for each restoration step.

The restoration of the faults in the proximal fault exposure are referred to steps a to h (Figure 26). We refer the restoration of the faults in the distal exposure to the same numbered steps except include subscripts for the intervening times between the proximal steps (Figure 27). Thus steps labeled g1, g2, and g3 refer to three time steps between the restored step f and h in the proximal set. The hanging wall of Fault-set C is repeated in the restoration of the distal fault set for comparison and reference.

Step A

In Figure 26A, the final restored section is the pre-growth heterolithic sands and shales. The light dashed lines in the figure show the locations of the future faults cutting the section (Figure 26B). A similar restoration is not provided for the distal fault set because the pre-growth section is mostly covered.

Step B

The first faults active in the deformation are Fault-set A and Fault-set C in the proximal mapped section. Two closely spaced fault pairs accommodate the displacement in each fault set. Contemporaneous displacement across synthetic fault pairs is common in normal faults and usually indicates the geometry of overlapping fault tips in map view. These overlaps are known as relay ramps or transfer zones (Peacock and Sanderson, 1991, 1994).

The thick SS1 sand fills the broad hanging walls of the early growth faults. The measured sections show large cross-beds in the sands close to Fault-set A, but a more flat stratified sand across Fault-set C. This observation is consistent with a broad flat hanging wall in Fault-set C that extends across the outcrop. SS1 is interpreted as an unfaulted thick sandstone in the distal mapped outcrop (Figure 27B).

Contemporaneous with the deposition of SS1 across Fault-set A and C, we interpret a set of antithetic faults bounding a horst in the footwall of Fault-set C (Figure 26C). SS1 is either eroded or not deposited over the horst crest. The exposure in the horst is poor, but detailed mapping shows that some of the pre-growth section is mechanically thinned by small-scale faulting over the crest.

Step C

Figure 26C shows continued thickening of the SS1 sands across the bayward dipping growth faults and the antithetic faults bounding the horst. Fault-set A and the antithetic faults define a broad graben in the proximal mapped section.

One interpretation of this early, restored state is that the SS1 sand is a pre-growth, prograding delta sand that is later faulted and eroded. Alternatively, the sand may have been deposited as a hanging wall sand in Fault-set A and then later displaced across Fault-set C and the antithetic faults. This interpretation is consistent with the nearly uniform bed thickness along the length of the outcrop, but is difficult to differentiate from a growth interpretation based on the exposure.

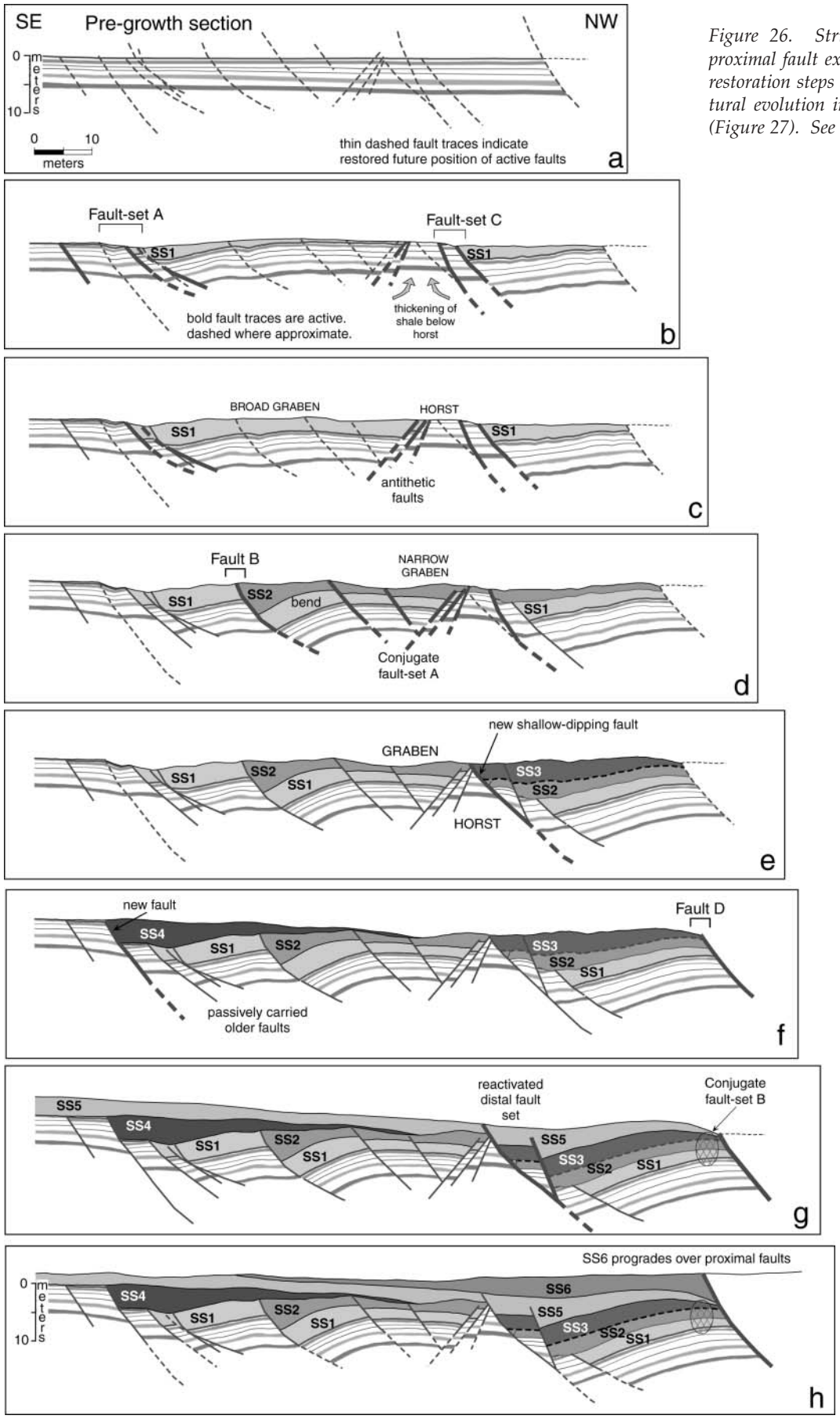

Figure 26. Structural restoration of the proximal fault exposure. The gaps between restoration steps are referenced to the structural evolution in the distal fault exposure (Figure 27). See text for details.

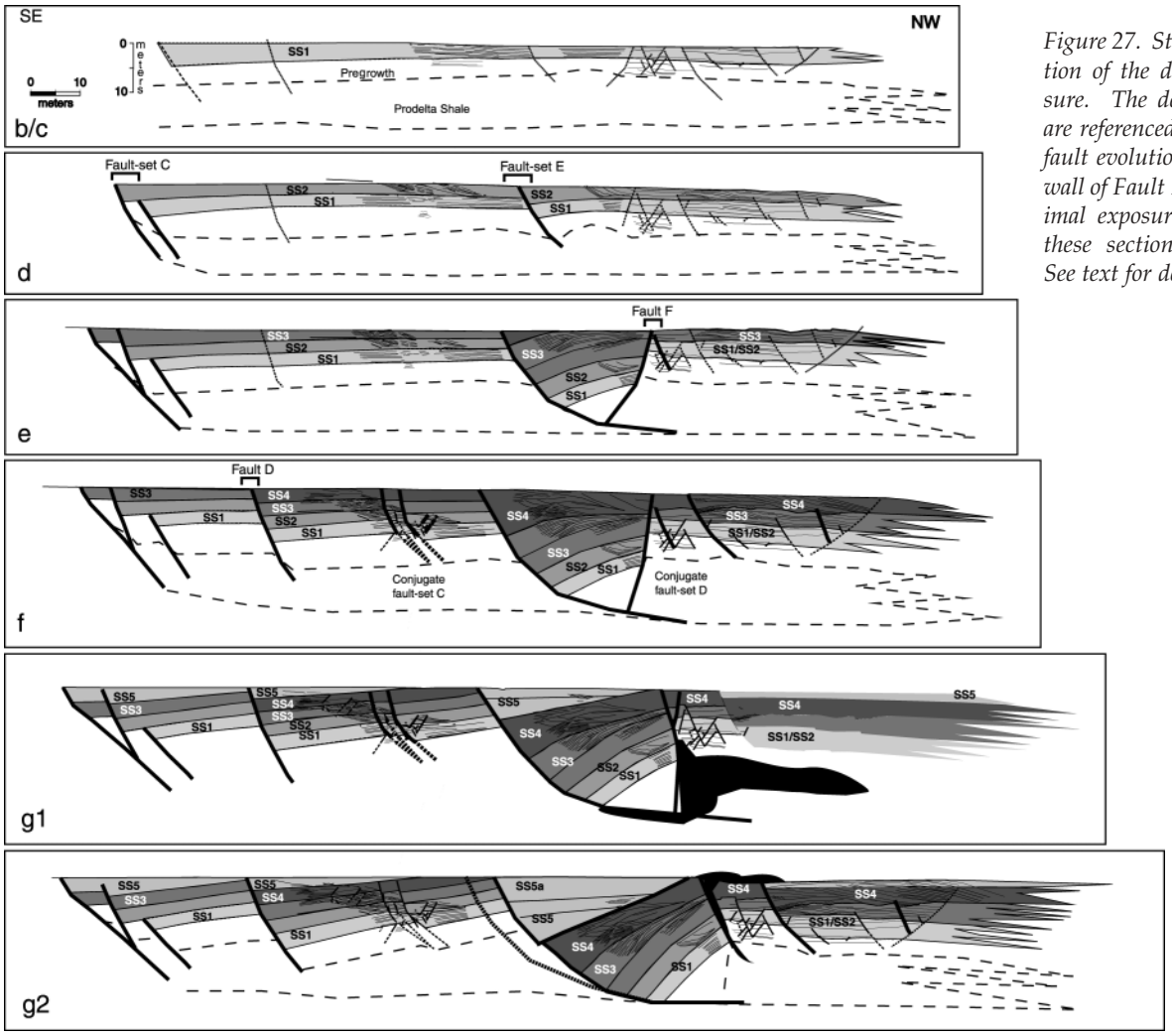

Figure 27. Structural restoration of the distal fault exposure. The deformation steps are referenced to the proximal fault evolution. The hanging wall of Fault D from the proximal exposure is repeated in these sections for reference. See text for details.

Step D

At the next step in the deformation (Figure 26D), displacement ceases on Fault-set A and is transferred to Fault B, which cuts the broad graben bounded to the northwest by the antithetic faults of the conjugate fault-set A. The cross-bedded sand SS2 thickens across Fault B and the antithetic faults. Fault B is strongly curved which results in a strongly curved hanging wall. Small throw synthetic faults develop in response to this bending and together with the antithetic faults form the conjugate Fault-set A (McClay, and Ellis, 1987; McClay and Scott, 1991; Brewer and Groshong, 1993).

The distal fault in the active growth fault pair of Fault-set C is inactive at this stage, and SS2 thickens across the more proximal fault in the set. The distal set in the pair is buried with deposition and growth across the fault.

At this stage in the deposition, the earliest fault displacement is interpreted in the more distal interpreted exposure with thickening of SS2 across Fault F (Figure 27D).

Steps E and F

During the next step in the deformation in the proximal mapped exposure, the most landward fault in Fault-set C cuts back into the footwall section or horst at a shallow angle beheading and offsetting the antithetic fault-set (Figure 26E). The other faults in Fault-set C are inactive and sand SS3 fills the hanging wall of the active fault.

Figure 26F shows displacement on the most landward fault in Fault-set A in the later step f. This fault cuts the shallowest section of all faults in this local set. We interpret the cross bedded SS4 sands, filling the hanging wall of this fault, as separate from the more distal SS3 sands which show abundant soft-sediment deformation and contorted bedding. This local deformation is unique in the section and, therefore, we interpret the SS3 sand as different from SS4, although it is possible that these sands are related and deposited contemporaneously. The similarity in the cross-bedded growth sands across much of the outcrop precludes a unique description across some fault blocks.

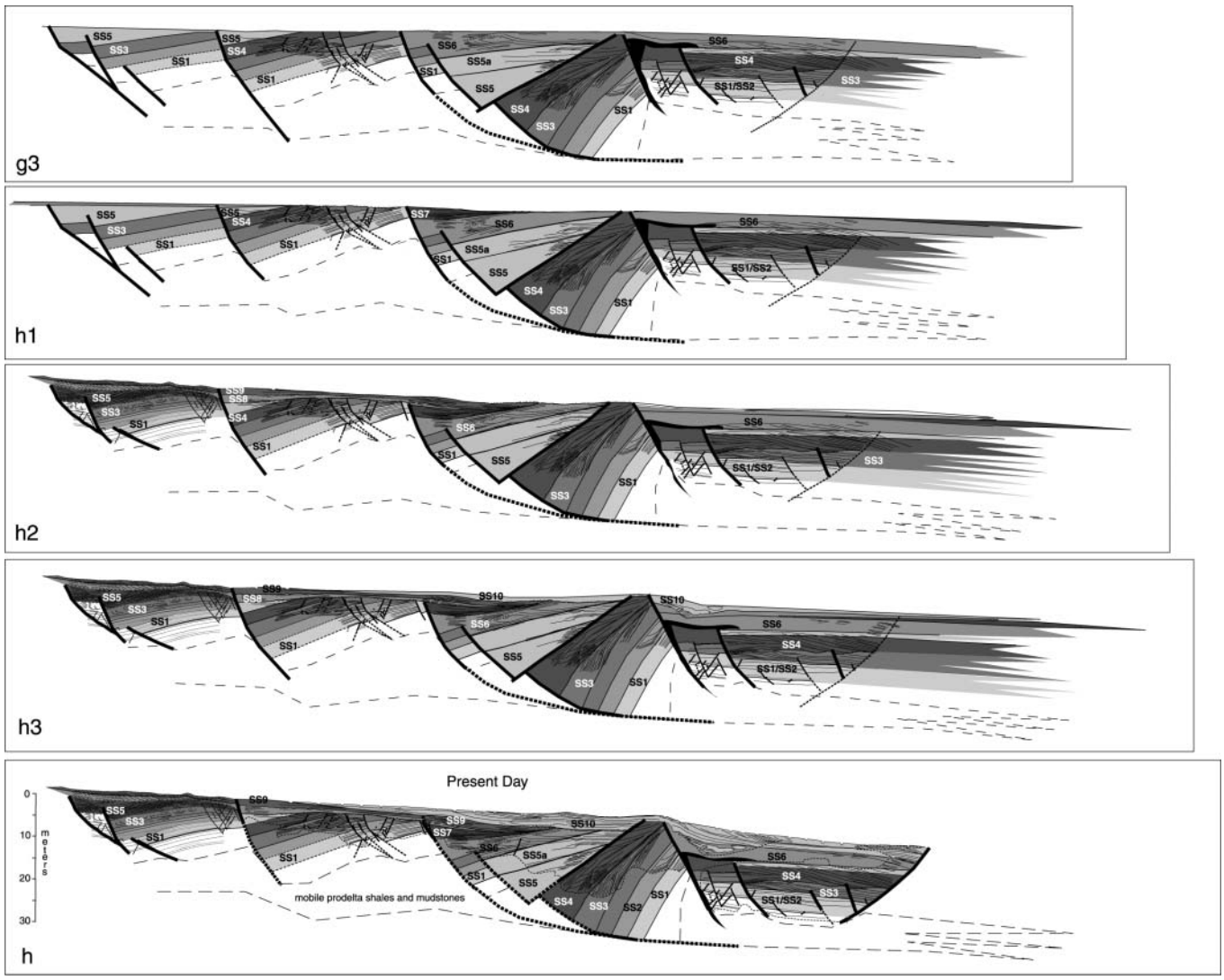

In the distal mapped exposure, the distal equivalent of these sands fills a local graben formed by Fault-set E and Fault F (Figure 27E). At this stage in the deformation Fault F is dipping to the southeast and is antithetic to Fault-set E. The faults together form a conjugate fault pair bounding a wide graben. Deposition across the faults fills the graben with thick sand sections that are only slightly thicker across the northwest dipping fault, which has a greater displacement. Rotation of the beds in the distal graben bound by Fault-set E and Fault F exposes the trailing ends of the beds, which are eroded.

Sand is either not deposited on the most distal flat lying beds in the distal exposure or the beds are uplifted and eroded (Figure 27E). We expect that both of these processes occur limiting the thickness of the sand beds in this distal location.

The first increment of displacement across Fault D at the boundary between the proximal and distal exposure occurs during the deformational step f (Figure 27F) with sand labeled SS4 filling the hanging wall. The sand is numbered sequentially from the underlying section to provide consistency to the distal mapped set of faults, although these sands may correlate with SS3 as discussed above. The bending of the hanging wall section with fault displacement nucleates the Conjugate fault-set C (McClay, and Ellis, 1987; McClay and Scott, 1991; Brewer and Groshong, 1993). During this stage in the structural evolution, the SS4 sandstones thicken dramatically across Fault-set E near the center of the distal exposure (Figure 27F).

Step G

The final fault growth in the proximal mapped exposure during step G shows displacement across the two proximal faults comprising Fault-set C and corresponding fill by the prograding SS5 sand (Figure 26G). These faults may have been active continuously throughout the deformation, as explained above, if the SS3 sand was deposited contemporaneously with SS4. The most bayward fault in the set terminates within SS5, but the most landward fault extends to the top of the sand.

Steps g1 to g3 in Figure 27 show the incremental complex deformation in the distal exposure during this stage of the structural evolution. The hanging wall of Fault D rotates with fault displacement accepting new growth sediment from sand SS5 and eroding the uplifted trailing edge of the older sands. The Conjugate fault-set C remains active during this deformation.

The hanging wall of Fault-set E also continues to rotate, but with more dramatic consequences. The fault displacement, responding to the layer extension, creates space in the hanging wall that is filled by sands SS5 to SS6, which are unique to the distal map exposure.

The rotation of the hanging wall reorients Fault F to a northwest dip (Figure 27 g2). The strong rotation and displacement of the deeper beds most likely overpressures the underlying muds at the leading edge of the rotated block and forces the mud up the surface of Fault F. Whether these muds ever reached the surface is questionable.

We expect that the unique geometry of steeply rotated beds extending deeply into the hanging wall of Fault E limits the subsequent motion of these beds. Continued fill within the fault block is accommodated by displacement across the southeast-dipping, bed-parallel surface between SS4 and SS5. This creates intersecting conjugate faults defined by the bed-parallel fault and Fault-set E.

Step H

During the final stages of deformation, the set of offlapping, wedge-shaped prograding sands (SS8-SS10) fill local space created in the hanging walls by offset across the Fault D and Fault-set F (Figure 27 h1), by differential compaction in the hanging wall of the Fault-set F (Figure 27 h2), and by differential relief across the rotated hanging wall of Fault-set E (Figure 27 h3). The sands prograding over the distal edge of the rotated fault block collapse and fold due to the gravity instability created by the slope across Fault F. The muds in this section are due either to the muddy distal toes of the prograding sands or to clays injected up the fault plane or a combination of the two.

In summary, the restorations show a complex growth history with proximal and distal growth fault sets active contemporaneously. The more distal faults in the section, however, have a larger throw than the more proximal faults and therefore a thicker section of cross-bedded sands.

DISCUSSION

Two styles of fault growth fill are present across the mapped exposure. The earlier deposited and more deeply buried medium-scale cross-bedded sandstones (e.g. SS1-SS3, Figure 4, and SS1-SS7, Figure 5) lack mudstone clasts or scarp-collapse breccias, which suggests that topography on the faults was minimal. In the younger prograding sands in the distal exposure (e.g. SS8-SS10, Figure 5), the faulted topography was infilled with offlapping, upward coarsening successions containing some mudstones, suggesting that several meters of topography may have existed. The older growth strata show that deposition of sand was synchronous with fault movement and that the faults were uniformly initiated with the deposition of the cross-bedded sands. An understanding of where deposition of cross-bedded sands occurs in modern delta fronts may give clues as to where and how growth faults nucleate.

Studies of sand deposition in modern shoal-water river-dominated deltas show a highly complex system of bifurcating distributary channels with several orders of channel splitting (Van Heerden and Roberts, 1988). The “terminal” ends of shallow high-order distributary channel are "plugged" by distributary-mouth bars (Figure 3). These mouth bars, in turn, cause sand to be deposited immediately upstream. Eventually, frictional deceleration and instability cause distributary channels to avulse. Depositional loci thus change position at a variety of scales and may shift not only seaward, as the delta progrades, but also landward, as channel plugging causes upstream deposition. Sand may also be deposited laterally as channels migrate or avulse. As demonstrated here, the growth faults initiate in response to deposition of sand in this dynamic proximal delta front area. Because these depositional loci can locally switch and even migrate upstream, associated growth faults show a similar complex pattern of initiation and movement.

The earlier-formed faults are similar to the Namurian deltas described by Rider (1978), who suggested that growth faults form as a natural consequence of delta progradation. Denser sands are deposited over less-dense mobile prodelta muds. Although broader-scale studies of growth faults show that they form in a progressively seaward-stepping fashion, as delta sediments prograde over shelf muds (Evamy et al., 1978; Bruce, 1983), our data shows that in detail, faults are not initiated or formed in such a progressive fashion.

We suspect that some larger-scale growth faults that are infilled with shallow-water facies may initiate in a manner similar to that interpreted here, as suggested by Rider (1978). However, regional-scale deformation in deltas is invariably tied to settings adjacent to a shelf-slope break, such as in the Gulf of Mexico (e.g. Winker, 1982) or Niger delta (Evamy et al., 1978). Large-scale faulting is enhanced by gravity-driven slumping and sliding on the continental slope, and the presence of thick underlying overpressured muds or salt (e.g. Winker, 1982; Winker and Edwards, 1983; Martinsen, 1989; Pulham, 1993). Thinner underlying mobile muds and smaller slopes, such as occur in intracratonic settings or farther inboard on the continental shelf, allow

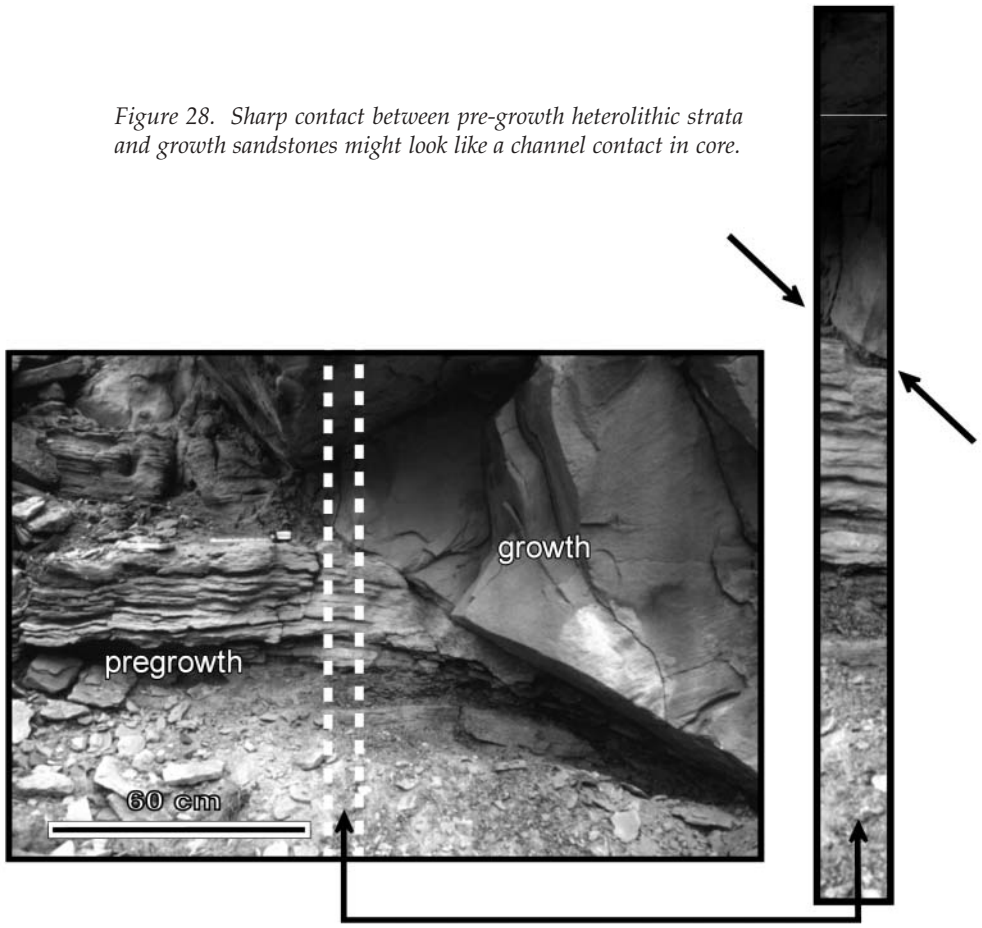

Figure 28. Sharp contact between pre-growth heterolithic strata and growth sandstones might look like a channel contact in core.

less accommodation for growth faulted strata (c.f. Brown, et al., 1973; Tye et al., 1999). Nevertheless, the observations of growth faults formed within a large shallow embayment of the Cretaceous seaway suggests that similar-scale features may be found in other river-dominated deltas deposited in shallow-water, intracratonic or shelf-perched, highstand settings. The main control on development of these growth strata appears to be extremely rapid sedimentation rates associated with highly river-dominated delta processes, rather than proximity to a shelf edge. Tectonic tilting likely formed this embayment. The active tectonic setting also likely caused earthquakes that may have been responsible for liquefying the prodelta mudstones of the Tununk, helping to initiate some of the faulting.

The younger faulting style is somewhat more similar to faults that form on a slope, such as the Cretaceous faults in Spitzbergen, documented by Nemec et al. (1988) and Pulham (1993). Muddy facies above the foundered block bounded by faults F and G (Figure 5) show large-scale deformation features, and may represent material that slumped away from the scarp formed during the movement along Fault F. Slumps naturally form on slopes because of downslope gravitational instability, which is enhanced where slope sediments are rapidly deposited and easily liquefied. Slumping occurs along faults and forms complex sea-floor topography. Deltas subsequently build over these areas and the faulted topography is filled with delta front turbidites and prodelta mudstones, such as is seen in SS10 (Figure 19). If a larger-scale slope existed, it is likely that fault F would evolve onto a regional-scale type feature.

Although these growth-faults show offset of a few meters, which is well below the scale of features typically imaged by conventional two-dimensional (2D) or three-dimensional (3D) seismic data, fault and fracture patterns often have a similar expression at a range of scales suggesting a self-similar geometry (Tchalenko, 1970). Regional-scale growth faults in areas such as the Niger delta or in the Gulf Coast of the U.S., show similar patterns of growth faulting to those documented here. It is also likely that the seismic-scale faults are associated or are formed of smaller-scale features, such as those documented here, but which may not be well imaged using conventional tools. Growth-faulted strata at a scale similar to that mapped in this study have been described with limited data in other shallow-water, river-dominated fluvial-deltaic reservoirs such as the supergiant Prudhoe Bay field in Alaska (Tye et al., 1999). In these types of fields, the interpretation of complex 3D geometry is incomplete. Use of these outcrop analogs should be considered in placement of horizontal production wells and to explain anomalous production. Local over-thickening of sandstones may provide addi-

tional reserves that may be missed in reservoirs delineated on the basis of conventional seismic surveys or widely spaced well logs. Evidence for small-scale synsedimentary growth faulting may be found in dipmeter logs, borehole imaging logs, or in cores, which can be compared to the facies and dip-changes, documented in this outcrop study. As one example, in core, the sharp contact between growth and pre-growth strata across a dipping fault might be misinterpreted as a channel margin (Figure 28). Because these synsedimentary faults form near the surface in soft sediment, features like fracture-filling cement and cataclastic features that commonly characterize late-stage tectonic faults are absent.

CONCLUSIONS

1. Early-formed growth faults initiated with deposition of dense, cross-bedded sands in shallow water (less than a few meters-deep), terminal distributary channels and distributary-mouth bars. Changes in the position of active faults through time reflect shifting depositional loci within the dynamic proximal delta front environment.
2. Later foundering of fault blocks results in an uneven sea-floor topography, which is more passively filled and smoothed over by progradation of shallow water deltas.
3. Growth faulting is accommodated by deformation and movement associated with dense sand loading underlying rapidly deposited, less-dense mobile prodelta shales. These types of shales are typical of those formed in highly river-dominated deltas. The lack of waves and tidal features is consistent with deposition of this portion of the Ferron into a protected embayment.
4. Detailed examination of the fault zones shows that deformation was largely by soft-sediment mechanisms, such as grain rolling and by lubrication of liquefied muds, causing shale smears. Mechanical attenuation of thin beds occurs by displacement across multiple closely spaced small throw faults.
5. Faults do not follow a systematic seaward or landward progression, which reflect the highly variable sedimentation patterns. Locally, faults within closely spaced fault sets step landward as they cut younger section.
6. Although fault blocks are reactivated, individual faults are rarely reactivated. Instead, new faults are formed during subsequent filling of the fault blocks. A single, through-going, long-lived fault was not mapped. Rather, complex sets of faults are active at different times.
7. Our results suggest that analog river-dominated deltaic subsurface reservoirs may be compartmentalized by growth faults, even in shallow-water, intracratonic, or shelf-perched highstand deltas. Reservoir compartmentalization would occur where thicker homogenous growth sandstones are placed against the muddy pre-growth strata and where faults are shale-smeared, and thus potentially sealing.

ACKNOWLEDGMENTS

We thank BP for providing financial support for this field work. Figures were drafted by Lou Bradshaw. We also thank reviewer Allan Driggs and editor Tom Morris who improved the clarity of the manuscript. This is contribution number 964 of the Geosciences Department, University of Texas at Dallas.

REFERENCES CITED

Berg, R. B., and A. H. Avery, 1995, Sealing properties of Tertiary growth faults, Texas Gulf Coast: AAPG Bulletin, v. 79, p. 375-393.

Bhattacharya, J. P., and R. G. Walker, 1992, Deltas, *in* R. G. Walker and N. P. James, eds., Facies models - response to sea-level change: Geological Association of Canada, p. 157–177.

Bishop, D. J., P. G. Buchanan, and C. J. Bishop, 1995, Gravity-driven, thin-skinned extension above Zechstein Group evaporites in the western central North Sea - an application of computer-aided section restoration techniques: Marine and Petroleum Geology, v. 12, p. 115-135.

Brewer, R. C., and R. H. Groshong, Jr., 1993, Restoration of cross-sections above intrusive salt domes: AAPG Bulletin, v. 77, p. 1769-1780.

Brown, L. F., Jr., A. W. Cleaves, II, and A. W. Erxleben, 1973, Pennsylvanian depositional systems in North-Central Texas - a guide for interpreting terrigenous clastic facies in a cratonic basin: Bureau of Economic Geology Guidebook No. 14, University of Texas at Austin, 122 p.

Bruce, C., 1983, Shale tectonics, Texas coastal area growth faults, *in* A. W. Bally, ed., Seismic expression of structural styles: AAPG Studies in Geology No. 15, p. 2.3.1-2.3.1-6.

Busch, D. A., 1975, Influence of growth faulting on sedimentation and prospect evaluation: AAPG Bulletin, v. 59, p. 217-230.

Diegel, F. A., J. F. Karlo, D. C. Schuster, R. C. Shoup, and P. R. Tauvers, 1995, Cenozoic structural evolution and tectono-stratigraphic framework of the northern Gulf Coast continental margin, *in* M. P. A. Jackson, D. G. Roberts, and S. Snelson, eds., Salt tectonics: a global perspective: AAPG Memoir 65, p. 109-151.

Dula, W. F., Jr., 1991, Geometric models of listric normal faults and rollover folds: AAPG Bulletin, v. 75, p. 1609-1625.

Edwards, M. B., 1976, Growth faults in upper Triassic deltaic sediments, Svalbard: AAPG Bulletin, v. 60, p. 341-355.

Elliot, T., and K.O. Lapido, 1981, Syn-sedimentary gravity slides (growth faults) in the coal measures of South Wales: Nature, v. 291, p. 220-291.

Evamy, D. D., J. Haremboure, P. Kamerling, W. A. Knapp, F. A. Molloy, and P. H. Rowlands, 1978, Hydrocarbon habitat of Tertiary Niger delta: AAPG Bulletin, v. 62, p. 1-39.

Fisher, Q. J., and R. J. Knipe, 1998, Fault sealing processes in siliciclastic sediments, *in* G. Jones, Q. J. Fisher, and R. J. Knipe, eds., Faulting, fault sealing and fluid flow in hydrocarbon reservoirs: Geological Society, London, Special Publication 147, p. 117-134.

Galloway, W. E., D. K. Hobday, and K. Magara, 1982, Frio Formation of Texas Gulf Coastal plain - depositional systems, structural framework and hydrocarbon distribution: AAPG Bulletin, v. 66, p. 649-688.

Gardner, M., 1995, Tectonic and eustatic controls on the stratal architecture of mid-Cretaceous stratigraphic sequences, central western interior foreland basin of North America, *in* S. L. Dorobek and G. M. Ross, eds., Stratigraphic evolution of foreland basins: SEPM Special Publication 52, p. 243-281.

Gingras, M. K., J. A. MacEachern, and S. G. Pemberton, 1998, A comparative analysis of the ichnology of wave- and river-dominated allomembers of the Upper Cretaceous Dunvegan Formation: Bulletin of Canadian Petroleum Geology, v. 46, p. 51-73.

Lindsay, N. G., F. C. Murphy, J. J. Walsh, and J. Watterson, 1993, Outcrop studies of shale smears on fault surfaces: International Association of Sedimentologists Special Publication 15, p. 113-123.

Martinsen, O. J., 1989, Styles of soft-sediment deformation on a Namurian (Carboniferous) delta slope, Western Irish Namurian basin, Ireland, *in* M. K. G. Whateley and K. T. Pickering, eds., Deltas - sites and traps for fossil fuels: Oxford, Blackwell Scientific Publications, Geological Society Special Publication 41, p.167-177.

McClay, K. R., and P. G. Ellis, 1987, Geometries of extensional fault systems developed in model experiments: Geology, v. 15, p. 341-344.

McClay, K. R., and A. D. Scott, 1991, Experimental models of hanging wall deformation in ramp-flat listric extensional fault systems: Tectonophysics, v. 188, p. 85-96.

Moslow, T. F., and S. G. Pemberton, 1988, An integrated approach to the sedimentological analysis of some lower Cretaceous shoreface and delta front sandstone sequences, *in* D. P. James and D. A. Leckie, eds., Sequences, stratigraphy, sedimentology; surface and subsurface: Canadian Society of Petroleum Geologists Memoir 15, p. 373 - 386.

Morris, T. H., and T. L. Nix, 2000, Structural and sedimentologic elements of an evolving growth fault system: outcrop and photomosaic analysis of the Ferron Sandstone, Utah (abs.): AAPG Annual Convention, Abstracta with Program, v. 9, p. A84.

Nemec, W., R. J. Steel, J. Gjelberg, J. D. Collinson, E. Prestholm, and I. E. Oxnevad, 1988, Anatomy of a collapsed and re-established delta front in Lower Cretaceous of Eastern Spitsbergen - gravitational sliding and sedimentation processes: AAPG Bulletin, v. 72, p. 454-476.

Nix, T. L., 1999, Detailed outcrop analysis of a growth fault system and associated structural and sedimentological elements, Ferron Sandstone, Utah: Master's thesis, Brigham Young University, Provo, 48 p.

Peacock, D. C. P., and D. J. Sanderson, 1991, Displacements, segment linkage and relay ramps in normal fault zones: Journal of Structural Geology, v. 13, p. 721-733.

—1994, Geometry and development of relay ramps in normal fault systems: AAPG Bulletin, v. 78, p. 147-165.

Pulham, A. J., 1993, Variations on slope deposition, Pliocene-Pleistocene, offshore Louisiana, Northeast Gulf of Mexico, *in* P. Weimer and H. W. Posamentier, eds., Siliciclastic sequence stratigraphy, recent developments and applications: AAPG Memoir 58, p. 199-233.

Rider, M. H., 1978, Growth faults in Carboniferous of Western Ireland: AAPG Bulletin, v. 62, p. 2191-2213.

Ryer, T. A., 1984, Transgressive-regressive cycles and the occurrence of coal in some Upper Cretaceous strata of Utah, U.S.A.: International Association of Sedimentologists Special Publication 7, p. 217-227.

Ryer, T. A., and M. McPhillips, 1983, Early Late Cretaceous paleogeography of east-central Utah, *in* M. W. Reynolds and E. D. Dolly, eds., Mesozoic paleogeography of west-central United States Rocky Mountain section: SEPM Symposium 2, p. 253-271.

Tchalenko, J. S., 1970, Similarities between shear zones of different magnitudes: Bulletin of the Geological Society of America, v. 81, p.1625-1640.

Tye, R. S., J. P. Bhattacharya, J. A. Lorsong, S. T. Sindelar, D. G. Knock, D. D. Puls, and R. A. Levinson, 1999, Geology and stratigraphy of fluvio-deltaic deposits in the Ivishak Formation - applications for development of Prudhoe Bay field, Alaska: AAPG Bulletin,

v. 83, 1588-1623.

Van Heerden, I. L., and H. H. Roberts, 1988, Facies development of Atchafalaya delta, Louisiana - a modern bayhead delta: AAPG Bulletin, v. 72, p. 439-453.

Winker, C. D., 1982, Cenozoic shelf margins, northwestern Gulf of Mexico: Transactions - Gulf Coast Association of Geological Societies, v. 32, p. 427-448.

Winker, C. D., and M. B. Edwards, 1983, Unstable progradational clastic shelf margins, *in* D. J. Stanley and G. T. Moore, eds., The shelfbreak - critical interface on continental margins: SEPM Special Publication 33, 139-157.

Yielding, G., G. Freeman, and B. Needham, 1997, Quantitative fault seal prediction: AAPG Bulletin, v. 81, p. 897-917.